AFRL-ML-WP-TR-2000-4137

A SURVEY OF THE PROPERTIES OF POLYION MULTILAYER THIN FILMS PREPARED BY THE SPONTANEOUS ADSORPTION TECHNIQUE

DR. TOM COOPER

AFRL/MLPJ
3005 P STREET BUILDING 651
WRIGHT-PATTERSON AFB, OH 45433-7702

OCTOBER 2000

FINAL REPORT FOR PERIOD MARCH 1993 – AUGUST 1997

APPROVED FOR PUBLIC RELEASE; DISTRIBUTION UNLIMITED.

MATERIALS & MANUFACTURING DIRECTORATE
AIR FORCE RESEARCH LABORATORY
AIR FORCE MATERIAL COMMAND
WRIGHT-PATTERSON AIR FORCE BASE, OH 45433-7702

NOTICE

When Government drawings, specifications, or other data are used for any purpose other than in connection with a definitely Government-related procurement, the United States Government incurs no responsibility or any obligation whatsoever. The fact that the Government may have formulated or in any way supplied the said drawings, specifications, or other data, is not to be regarded by implication, or otherwise in any manner construed, as licensing the holder, or any other person or corporation; or as conveying any rights or permission to manufacture, use, or sell any patented invention that may in any way be related thereto.

This report is releasable to the National Technical Information Service (NTIS). At NTIS, it will be available to the general public, including foreign nations.

This technical report has been reviewed and is approved for publication.

Thomas M. Cooper

THOMAS COOPER, Scientist
Agile Limiters
Hardened Materials Branch

William D. Cowan

WILLIAM D. COWAN, LtCol, USAF, Chief
Hardened Materials Branch
Survivability and Sensor
Materials Division

William R Woody

WILLIAM R. WOODY, Chief
Survivability and Sensor
Materials Division

If your address has changed, if you wish to be removed from our mailing list, or if the addressee is no longer employed by your organization please notify AFRL/MLPJ, Wright-Patterson AFB, OH 45433-7702 to help maintain a current mailing list.

Copies of this report should not be returned unless return is required by security considerations, contractual obligations, or notice on a specific document.

REPORT DOCUMENTATION PAGE

FORM APPROVED
OMB NO. 0704-0188

1. AGENCY USE ONLY *(Leave Blank)*	2. REPORT DATE	3. REPORT TYPE AND DATES COVERED
	October 2000	March 1993 - August 1997

4. TITLE AND SUBTITLE
A Survey of the Properties of Polyion Multilayer Thin Films Prepared by the Spontaneous Adsorption Technique

5. FUNDING NUMBERS
PE 62102F
PR 2422
TA 02
WU FJ

6. AUTHOR(S)
Thomas M. Cooper

7. PERFORMING ORGANIZATION NAME(S) AND ADDRESS(ES)
AFRL/MLPJ
3005 P Street Building 651
Wright-Patterson AFB, OH 45433-7702

8. PERFORMING ORGANIZATION REPORT NUMBER

9. SPONSORING MONITORING AGENCY NAME(S) AND ADDRESS(ES)
Materials And Manufacturing Directorate
Air Force Research Laboratory
Air Force Materiel Command
Wright-Patterson Air Force Base, OH 45433-7318
POC: Thomas Cooper, AFRL/MLP, 937-255-3808 x3157

10. SPONSORING/MONITORING AGENCY REP NUMBER
AFRL-ML-WP-TR-2000-4137

11. SUPPLEMENTARY NOTES

12a. DISTRIBUTION/AVAILABILITY STATEMENT
Approved for public release; distribution unlimited.

12b. DISTRIBUTION CODE

13. ABSTRACT

The Spontaneous Adsorption technique is a low cost approach for assembling interesting thin films. Virtually any polyion can be incorporated into a film, including dyes, polymers, proteins, viruses, inorganic nanoparticles and ceramic plates. The technique is simple to automate. The SA technique requires minimum equipment investment and interesting films can be made by hand with beakers, electrolytes, water and a stopwatch. By using a moderately-priced automated slide stainer, complex multilayers can be prepared. Compared to the LB technique, scaleup of automated SA film assembly is less costly. This report contains numerous examples of PMFs whose properties can be tuned by varying the number of layers or the spacing between functional layers. Virtually any substrate upon which a charge can be placed can be used in the SA process. The SA process exhibits self-healing characteristics. Point defects and dust inclusions have limited propagation distance. Varying bilayer thickness can be obtained by changing the ionic strength. The SA technique can be combined with other methods (Langmiur-Blodgett technique, spin coating, etc.) to provide a variety of films.

14. SUBJECT TERMS
Polyion Multilayer Thin Film, Spontaneous Adsorption (SA), Biomimetic Thin Film, Polymer Science

15. NUMBER OF PAGES
81

16. PRICE CODE

17. SECURITY CLASSIFICATION OF REPORT	18. SECURITY CLASSIFICATION OF THIS PAGE	19. SECURITY CLASSIFICATION OF ABSTRACT	20. LIMITATION OF ABSTRACT
UNCLASSIFIED	UNCLASSIFIED	UNCLASSIFIED	SAR

Standard Form 298 (Rev 2-89)
Prescribed by ANSI Std Z39-18
298-102

A Survey of the Properties of Polyion Multilayer Thin Films Prepared by the Spontaneous Adsorption Technique

by

Thomas M. Cooper

Air Force Research Laboratory
Materials Directorate
AFRL/MLPJ
3005 P St. Ste 1
Wright-Patterson Air Force Base, OH 45433
Ph: 937-255-3808 x3157
Fax: 937-255-1128

E-Mail: Thomas.Cooper@afrl.af.mil

Table of Contents

I. Introduction

Biomimetics is defined as "the study of biological structures, their functions and their synthetic pathways in order to stimulate new ideas and to develop these ideas into synthetic systems similar to those found in biological systems"[1]. It is a strategy for designing complex, multifunctional materials having the capacity for supramolecular self-assembly, conversion between chemical, thermal, mechanical, electromagnetic and electrical energy and the ability to sense and adapt to the environment[2, 3]. Synthetic materials having these characteristics are called "smart materials"[4]. Biological systems and materials have hierarchical organization. In the context of materials science, Di Marzio defines hierarchical structure as an "assemblage of assemblages" that include scale, interaction between assemblages and architecture[5]. Hierarchical systems abound in biology. A survey of common systems and their relation to design of new materials has been described in a recent monograph[6]. An example given is the tendon, where the levels of structural hierarchy and fiber diameter are: collagen polypeptide(0.5 nm) $\rightarrow$triple helix(1.5 nm) $\rightarrow$ microfibril(3.5 nm) $\rightarrow$ subfibril(10-20 nm) $\rightarrow$ fibril(50-500 nm)$\rightarrow$ fascicle(50-300 μm) $\rightarrow$ tendon(0.1-0.5 mm). Other examples given include wood and a diarthroidial joint, each with six levels of structural hierarchy. Many of the components of a biological system have the capacity to undergo self-assembly. Self-assembly is "self-organization of many identical, or nearly identical subunits" [5]. Phase transitions leading to self-assembled systems, include the helix-to-coil transition, adsorption onto a surface, liquid crystal transitions and membrane formation. This report gives examples of multilayers in self-assembly(Section IIA), biology(Section IIIA) and the biomineralization process(Section IIIB).

Biomimetics can be applied to the development of unique thin films. A novel film formation technique has been described which mimics aspects of the sequential adsorption of materials onto a surface observed in biomineralization. Several review articles have recently been published describing sequential adsorption and related thin film preparation techniques[7-11]. Films prepared by this technique have many names given in the literature focusing on the completed film or the film preparation process, including fuzzy nanoassemblies[7], polyion multilayers[12], alternate polyelectrolyte thin films[13], alternate assembly[14], alternate adsorption[15], molecular deposition films[16], alternate layer-by-layer assembly[17], layer-by-layer deposition[18], bolaform amphile multilayers[19], alternating multilayer films[20], polymer self-assembly solution adsorption[21], multilayers of polyelectrolytes[22], multilayer films[23], layered composite films[24], self-assembled alternating multilayers[25], layer-by-layer self assembly[26], molecular deposition[27], reactive self-assembly[28], self-assembled polymer thin films[29], molecular self-assembly[30], molecular beaker epitaxy[31], nanoparticle

heterostructures[32], polycation/polyanion self-assembly[33], sequential adsorption[34], stepwise assembly[35], ultrathin polyelectrolyte films[36], ultrathin film based on electrostatic interaction[37] and electrostatic self assembly[38]. In this report the film-forming process will be called sequential adsorption(SA). A polyion-containing film prepared by SA will be called "polyion multilayer film"(PMF). This report reviews the literature on PMFs prepared by the SA technique published prior to August, 1997. Films containing polymers, dyes, amphiphiles, inorganic compounds, colloids and proteins are described as well as guidance on preparation and characterization of PMFs.

II. Examples of Supramolecular Complexes in Biology and Polymer Science

A. Thermodynamics and Kinetics of Self-Assembly

Formation of biological thin films includes self-assembly of macromolecular complexes. Certain macromolecules have the ability to spontaneously form complex structures. Examples of these processes in thin film formation include coil-to-helix formation upon adsorption onto a surface[38], formation of the biotin-streptavidin complex[39] and antigen-antibody interactions[20]. S layer proteins are an example of a protein forming an ordered two-dimensional array on a surface[40]. A simple model of linear assembly processes leading to filaments has been described by Engel[41]. In the first step, two monomers dimerize

$$A+A \rightleftharpoons A_2 \qquad (1)$$

Polymerization to a linear aggregate occurs by addition of monomer to the filament

$$A_{i-1} + A \rightleftharpoons A_i \qquad (2)$$

By analogy to the helix to coil transition, the initial dimerization step is a nucleation process with subsequent propagation steps with equilibrium constants

$K_2 = \sigma K$ (nucleation) (3)

$K_i = K$ (i 3) (propagation). (4)

The cooperativity parameter σ is small($\sigma << 1$), with subsequent propagation steps being thermodynamically favorable($K >> 1$). The monomer concentration c_1

will always be smaller than a critical concentration $c_{crit} = K^{-1}$. When performing a self-assembly experiment the total (monomer + aggregate) concentration c_0 is varied. Below c_{crit}, monomer concentration increases with c_0. Aggregate formation only occurs above c_{crit}. Engel gives an example of "all or nothing" behavior in the association of actin. The cooperativity parameter σ is 2×10^{-7} and the equilibrium constant for the propagation step is $K = 1.7 \times 10^5\ M^{-1}$. Filaments form only above $c_{crit} = 5.88\ \mu M$.

In a similar manner the kinetics of self assembly follow a mechanism involving slow dimer formation as a nucleation step followed by faster propagation steps. In his review article, Engel describes the kinetics of polysheath formation. The kinetics follow a sigmoidal growth curve with the slow bimolecular nucleation rate constant being $k_N = 10^{-2}\ M^{-1}s^{-1}$ and the rapid propagation bimolecular rate constant being $k = 10^5\ M^{-1}s^{-1}$.

B. Examples of Self-Assembly in Protein and Polymer Systems

Tropomyosin provides a well-understood example of a protein that undergoes self-assembly processes(Fig. 1)[42].

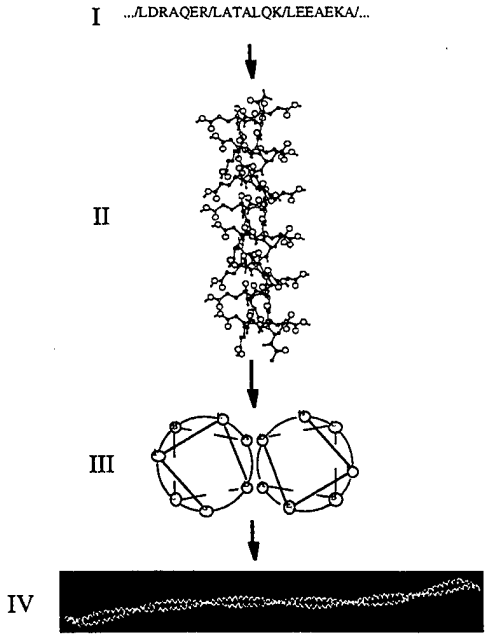

Figure 1. Example of self-assembly in tropomyosin. I: Three heptets of the tropomyosin amino acid sequence[43]. Amino acids in a heptet are labeled "abcdefg". II: Polypeptide chain self-assembles into an α-helix. III: Self-assembly into α-helix causes formation of hydrophobic regions in heptet positions a and d, and hydrophilic regions at heptet positions b, c, e, f and g. IV: Two tropomyosin helices self-assemble into coiled-coil.

Having a coiled-coil conformation, it belongs to the K-M-E-F(keratin, myosin, epidermin and fibrin) class of proteins. Its amino acid sequence has a seven-fold repeat pattern "abcdefg",

where amino acids in position a and d tend to have hydrophobic side chains, while those in positions b, c, e, f and g tend to be hydrophilic[43]. Because the amino acids tend to be helix formers, the polypeptide chain self-assembles into an α-helix. Upon formation of an α-helical conformation, a new, higher order structure forms on the surface of the helix. The hydrophobic amino acids in positions a and d form a hydrophobic band on the surface of the helix. The remainder of the surface contains the hydrophilic amino acids. Two tropomyosin monomers self-assemble into a coiled-coil dimer. The coiled-coil dimer forms numerous higher order structures, including filaments resulting from head-to-tail interactions and complex formation with its natural partner troponin[44, 45]. The tropomyosin-troponin complex aggregates with actin and myosin, forming muscle fibers.

Recent work has demonstrated self-assembly in synthetic polymer systems that mimic processes seen in proteins. Synthesis of a two dimensional polymer shaped as molecular sheets had been described[46,47]. The molecular precursor of the 2D polymers contains three subunits which contribute to the final morphology.

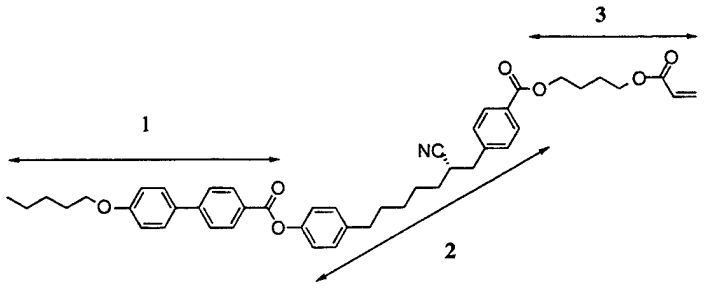

I

Fragment 1 is a alkyl biphenyl smectogen which promotes layer formation. Fragment 2 contains a chiral center with a strongly polar cyano group. Molecular recognition between the chiral units is possible. Upon heating the cyano groups polymerize to form imine bonds and the acrylates form poly(acrylate). Fragment 3 contains an acrylate group which can also polymerize with its neighbors. When only one of the functionalities are present, the oligomer polymerizes into a comb polymer. When both functionalities are present, the oligomer self-assembles into a layered structure where the cyano and the acrylate groups polymerize in different layers. The two dimensional polymer has a molecular weight on the order of 10^6 daltons and a monodisperse thickness of 5 nm. Electron micrographs of the two dimensional polymer shows self assembly of the sheets into stacks of sheets.

Another example from the same research group is the rodcoil[48, 49].

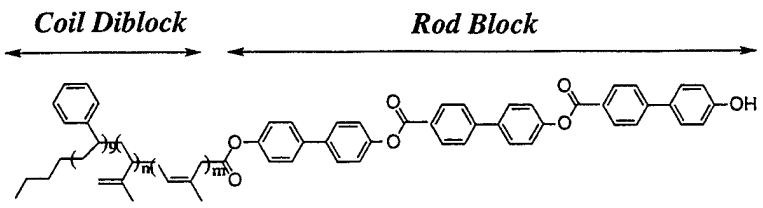

II

The oligomer precursors have three blocks. The first block consists of a styrene monomer polymerized with an average length of 9 monomer units. A second block with the same degree of polymerization contains isoprene units. The third block contains three biphenyl units. The oligomer behaves like a rod diblock linked to a coil block. When thin films of the triblock molecules are cast, arrays of nearly identical mushroom-shaped nanoaggregates formed, with approximately 100 molecules in each nanostructure. Contact angle and nonlinear optical measurements suggests the nanoaggregates stack in a noncentrosymmetric fashion.

C. Interpolyelectrolyte Complexes

Investigations of interpolyelectrolyte complexes(IPEC) give insight into the properties of structures held together by electrostatic forces. Kabanov has written a review of their properties[50]. The review article describes several Russian studies that give insight into the fundamental mechanism of multilayer deposition. When two aqueous solutions, one containing a polycation, the other a polyanion, are mixed, a complex forms.

$$(A^-b^+)_n + (B^+a^-)_m \rightleftharpoons (A^-B^+)_x + (A^-b^+)_{n-x} + (B^+a^-)_{m-x} + xa^- + xb^+$$

III

The conversion ratio $\theta = x/m$ when n m and $\theta = x/n$ when $n<m$. The ratio θ is a function of pH and ionic strength. The ratio $Z = m/n$. When $Z<1$, the IPEC will have a negative charge. When $Z>1$, the complex will have a positive charge. When $Z=1$, the complex will have no charge and be insoluble. Fluorescence quenching experiments were performed using pyrenyl-labeled polymethacrylate(PMA*) anions containing one laber per 350-1500 monomer units and (1-ethyl-4-vinylpyridinium)-vinylpyridine copolymer cations(PVPC) the 1-ethyl-4-vinylpyridinium units quench the fluorescence of the pyrenyl labels.

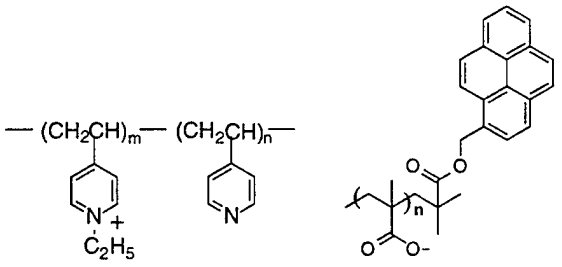

PVPC PMA*

IV-V

Through the use of stopped flow kinetics measurements, the fundamental complexation reaction is probably diffusion limited. The polyion exchange reaction has also been investigated

$$(PMA/PVPC) + PMA^* \rightleftharpoons (PMA^*/PVPC) + PMA$$

VI

In this experiment the bimolecular rate constant is of the order 10^4 - 10^6 l/mol-s, 3-5 orders of magnitude smaller than the diffusion rate constant. The result suggest the exchange reaction occurs through the formation of a ternary complex PMA*-PVPC-PMA resulting from the interpenetration of PMA-PVPC coils and PMA* coil. The rate constant increases dramatically with ionic strength, showing counterion charge shielding stabilizes the ternary complex. Enzymes have been placed in IPECs. Kabanov gives kinetic parameters of the enzyme penicillinamidase under various conditions. When bound to a PMA/PVPC IPEC, enzyme activity is nearly identical to the native preparation. When bound to celluose triacetate fibers or polyacrylamide gel, enzyme activity decreases 50-fold.

III. Examples of Multilayer Thin Films in Biology

A. Biological Structural Colors

There are numerous examples of optical thin films in biology that show a variety of optical phenomena. Structural colors in insects have been investigated for many years[51]. Original light microscope studies[52-54] drew a distinction between structural and pigment colors. Structural colors could be altered by physical means like pressure, swelling or shrinking or addition of an index-matching solvent. For example, ididescent wing membranes undergo a reversible color change upon addition of a swelling agent. These phenomena result from thin film optical interference. The white color seen in insect wings results from light scattering. In contrast, pigment colors are extractable by solvents. Recent electron microscopy investigations

give details about the source of the optical phenomena in insect wints. Structural colors appear in butterfly and moth scales and serve as thin film interference filters[55]. Each scale is a flattened stack with two surfaces, the upper and lower lamina, with a stalk attached to a socket on the wing(Fig. 2).

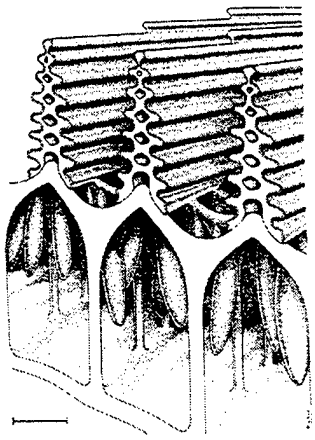

Figure 2. Image of a portion of an ultraviolet-reflecting scale of the male *Eurema lisa*. The laminate ridges projecting upward have ultraviolet reflecting capability. Ellipsoidal structures projecting downward are pigment granules giving a yellow color to the scale. Pillar-like trabeculae join the upper and lower lamina. Scale bar: 0.5 μm. Reprinted with permission from H. Ghiradella, D. Aneshansley, T. Eisner, R.E. Silberglied and H.E. Hinton *Science* **178**, 1214, (1972) Copyright 1972 American Association for the Advancement of Science.

The upper lamina, contains a grid consisting of raised longitudinal ridges regularly joined by cross-ribs. The ridges and cross-ribs form a series of windows opening into the scale interior. In the scale interior are pillars that serve as spacers between the lower and upper laminae. Pigment granules are found in the interior of the scale. In ridge-iridescent scales, the ridges contain microribs that form the reflective elements. The ridge structure is an alternating stack of high and low refractive index layers. Each ridge performs as a quarter-wave thin-film interference mirror with a phase change upon reflection.

The optical thickness(nt) of a dielectric stack layer composed of alternating thicknesses t_1 and t_2 and indices n_1 and n_2 is given by the relation

$$n_1 t_1 = n_2 t_2 \tag{5a}$$

and

$$n_1 t_1 + n_2 t_2 = nt \tag{5b}$$

where nt is the optical thickness of one bilayer composed of a high and low index component. Upon normal incidence, the wavelength of maximal reflection is given by

$$\lambda = 4n_1t_1 = 4n_2t_2 \quad (6a)$$

An alternative formulation is

$$\lambda = 2nt. \quad (6b)$$

For example, certain butterflies have ultraviolet-reflecting scales with an index of refraction n = 1.60 having microribs with 510 Å thickness with an 848 Å air space between them[56, 57]. If the system behaves as a quarter wavelength reflection filter, the layers should reflect light with a constructive interference maximum at 343 nm. Reflection spectroscopy measurements of scales show ultraviolet reflection with a maximum at 348 nm. The structures also change color when the scale tilts. The wavelength of maximal constructive interference varies from 320 to 348 nm over a wing tilt from 0 to 50 deg.

How are these structures formed? Ghiradella studied the development of iridescent scales from two lycaenid butterflies[58]. The two types of internal reflective structures are developmentally closely related. The diffraction lattice appears to form within the scale cell boundaries through the assistance of a convoluted series of membranes(Fig. 3).

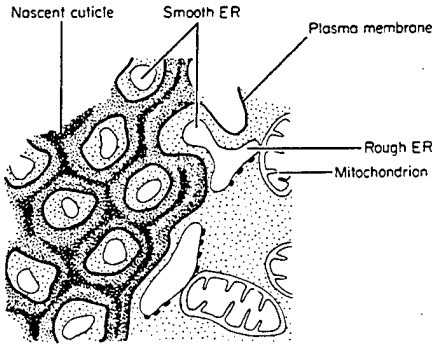

Figure 3. Sketch of developing scale of the butterfly *M. grynea.* The smooth endoplasmic reticulum(ER) buds off into the rough ER into a regular framework around which the membrane cuticle(MC) units form themselves into a reflective lattice. Reprinted by permission from H. Ghiradella *J. Morphology* **202**, 69, (1989), Copyright 1989 Wiley-Liss, Inc., a subsidiary of John Wiley &Sons, Inc.

The cell produces membrane-cuticle units which are continuous with the invaginations of the plasma membrane. The units aggregate, forming "crystallites that grow toward each other by accretion until the adult morphology arises." Formation of the thin-film interference laminae "result from the condensation of a network of filaments and tubes secreted outside boundaries of the cell." She hypothesizes that the lattice may form by a process within the scale cell where the cell produces a material which self-assembles to a face-centered cubic lattice. The thin film

laminae then form by stretching the lattice.

Structural colors have been found in plants. Iridescence in leaves have been observed in understory plants growing in shady areas of tropical rain forests[59-61]. For example, the leaf reflectance spectrum from *Lindsaea lucida* has a blue-green reflection band at 538 nm. The outermost cell wall of the adaxial epidermis contains helicoidal nests of arcs arranged in ranks separated by lamellae with a lamellar spacing(t) of 192 nm. Assuming a refractive index n=1.45, and a bilayer optical thickness of 278 nm, a reflectance maximum of 557 nm is calculated. Iridescent blue fruits of *Elaeocarpus angustifolius* have a reflection band at 439 nm[62]. Electron microscopy reveals a multilayer structure within the epidermis consisting of a parallel network of strands 78 nm thick. Thin film interference theory, assuming n=1.40, predicts an optical thickness of 109 nm and a calculated reflectance maximum of 436 nm.

B. Biomineralization

Detailed information about the mechanism of biomineralization in molluscs has been obtained through investigations of "flat pearls"[63]. By placing a glass substrate between the mantle and the inner surface of the mollusc shell, the process of biomineralization can be monitored *in vivo*. A schematic cross section of the outer edge of the shell of a red abalone is given in Fig. 4.

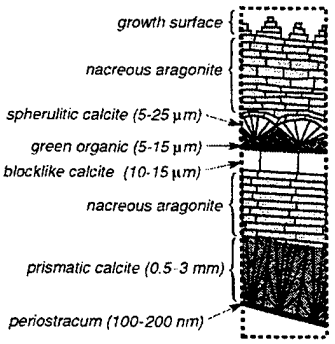

Figure 4. Schematic of a vertical section of the outer edge of the shell and mantle of a red abalone(*Haliotis rufescens*) The figure is not drawn to scale. Adapted with permission from reference [63]. Copyright 1996 American Chemical Society

Epithelial tissue lining the inner surface of the shell secretes shell precursors into the extrapallial space, a thin compartment between the mantle and inner shell surface. The shell structure contains multiple organic, calcite and aragonite layers. Growth of a flat pearl showed biomineralization begins with deposition of an organic sheet on the substrate, followed by growth of a calcite layer and an abrupt transiton to an aragonite layer. The biomineralization process was shown to be sensitive to substrate. Implantation of roughened glass coverslips or a

hydrophobic substrate caused deposition of regions of disorder in the calcite layer and with deposition of an organic sheet associatied with reinitiation of the biomineralization process. Soluble mollusc-shell proteins have been found which control crystal phase during nacre formation[64]. These proteins contain high proportion of aspartate, glycine, glutamate and serine residues with a $(asp\text{-}Y)_n$, with Y being primarly glycine[65]. Proteins were isolated from the aragonitic or the calcitic portions of the red abalone shell. Denaturing gel electrophoresis showed the aragonitic composite contains three proteins, while the calcitic portion contained six proteins. Calcium carbonate crystals were grown in the presence of these proteins. Crystals grown in the absence of soluble protein exhibited the rhombohedral calcite morphology. Crystals grown in the presence of the calcitic protein fraction had the spherulitic calcite morphology, while those grown in the presence of the aragonitic fraction formed aragonite needles in the plane of the nucleation layer. Addition of mineral-specific proteins induced the abrupt calcite-to-aragonite transition seen in abalone shell. Rhombohedral calcite crystals were exposed to a crystal growth medium containing the proteins. Addition of aragonitic polyanionic proteins caused aragonite needle growth, and addition of calcitic proteins caused calcite overgrowth. Sequential transition of calcite to aragonite and back to calcite was caused when soluble aragonite proteins were depleted, causing formation of calcite. In a related study, glycoproteins were isolated from mollusk shells and *in vitro* studies of the nucleation of calcium carbonate in the presence of the glycoproteins, chitin and silk fibrin, giving similar behavior[66]. Insight into the mechanism of aragonite tablet growth has been obtained through a recent AFM study[67]. Flat pearls were demineralized, leaving an iridescent patch of organic material. AFM and scanning ion conductance microscopy revealed the organic sheets had pores 5-50 nm in diameter. The results support a model where nacre formation occurs when mineral bridges form through the pores in the organic layers between the aragonite tablets.

Crystal synthesis analagous to the biomineralization process has been demonstrated[68]. They synthesized CdS in PEO thin films. The synthetic factors emphasized included strong binding by the matrix to the inorganic reagents, solubility of the reagents in the polymer matrix and an ordered, regular environment to induce nucleation. The CdS crystals prepared had uniform size, phase and crystallographic orientation. The crystals were in the "rock salt" morphology, a phase normally appearing at high temperatures.

IV. Biomimetic Thin Films Prepared by the Sequential Adsorption Technique

The composition, morphology and mechanism of formation of the structures that result in insect iridescence and plant structural colors are poorly understood. Because of the development of the flat pearl model system, the mechanism of mollusc shell biomineralization is

beginning to be clarified. Biomineralization in mollusk shells involves sequential laying down of organic layers that serve as templates for growth of specific calcium carbonate polymorphs above the layers and through the pores in the organic sheets. By changing the protein secreted by the secretory epithelium in the mantle, the crystal morphology can be altered in a controlled manner.

Aspects of the process of biomineralization can be mimicked for the synthesis of multilayer thin films. Iler described the process in the 1960's[69, 70]. He gives several examples of multilayer formation, including albumin/silica, silica/alumina, treatment of fabrics, multilayers on metal, and mica. The process is depicted in Fig. 5.

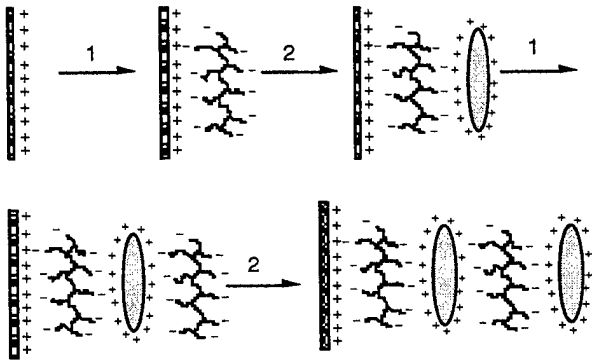

Figure 5. Schematic of SA process. A positively charged substrate is dipped into an aqueous solution containing a negatively charged polyelectrolyte(1). The negatively charged polyelectrolyte adsorbes onto the surface. Following rinsing and drying, the film is dipped into a solution containing a positively charged polyelectrolyte(2). This process can be repeated indefinitely with multiple electrolyte solutions.

A charged substrate is placed into a solution containing an oppositely charged polyelectrolyte. The polyelectrolyte adsorbs to the surface. Following a rinsing and drying step, the film is placed into another polyelectrolyte solution. The resulting film contains a multilayer with alternating oppositely charged monolayers. To the knowledge of the author, there has been no activity with this method until the early 1990's. An example of nomenclature used in this report follows. "S + $(A/B)_n$ + $(C/D)_m$" represents a substrate(S) upon which n A/B bilayers and m C/D bilayers have been placed. The order of adsorption is from left to right with the charge of subsequent layers determined by the charge of the substrate. When the substrate is not specified, it is implied in the text.

A. Procedure for Preparing Polyion Multilayer Films

1. Substrate Preparation

a. *Substrate Cleaning* Successful film formation requires clean substrates. Glass slides

are cleaned with a boiling solution of 7:3 mixture of concentrated H_2SO_4 and 30% H_2O_2 (Piranha solution) while stirring. The slides are then rinsed with a stream of deionized water and dried with N_2. The slides are then hydroxylated by dipping in a 10:3:3 solution of deionized water, 30% H_2O_2 and concentrated NH_4OH at room temperature 2-3 days. The slides are then dipped in a deionized water bath, rinsed with CH_3OH and dried with N_2 [38]. Gold coupons have been cleaned with Piranha solution, followed with a 20 min sonication with distilled water[71]. *Warning: These mixtures are corrosive and can cause severe burns. They react violently with many organic materials and should not be stored. Perform cleaning procedure in a fume hood while wearing suitable personal protective equipment.*

b. *Glass and Quartz* Although films can be prepared on an untreated surface[38], efficient film formation requires modification of the surface with charged groups. The following procedures have been used successfully, but details about kinetics and surface density of charged groups are not known. Positively charged surfaces have been made by letting a 5% solution of *N*-[3-(trimethyloxysilyl)propyl]ethylenediamine solution sit for 5 min to ensure silanol formation. The slides are then silanized for 10 min, followed by an ethanol rinse, a deionized water rinse, N_2 drying and 10 min cure in a vacuum oven[38]. Another example of use of this agent involves a 12 hour silanization in a 5% solution, followed by a 10 min toluene rinse, a 10 min 1:1 methanol/toluene rinse, a 10 min methanol rinse and a water rinse. Silanizations with 3-aminopropyltrimethoxysilane have been performed under a dry N_2 atmosphere to prevent oxidation to poly(dimethyoxysilane)[72]. Quartz plates washed in alkaline aqueous alcohol with sonication have negative charges resulting from partial hydrolysis of the surface[73]. A hydrophobic surface can be prepared by exposing glass slides to 1,1,1,3,3,3-hexamethyldisilazane at reduced atmospheric pressure(200 torr) for 36 hours[74].

c. *Gold* Gold surfaces have been used as substrates for PMFs[75]. Caruso exposes the gold surface to 1mM 3-mercaptopropionic acid-ethanol solution for 24 h, fillowed by a deionized water rinse and nitrogen drying. The carboxyl groups on the gold surface are ionized at pH 8. He advises careful choice of film deposition time, as exposure of the coated gold substrate causes deterioration of the gold surface. Sulfonic acid groups have been added to a gold surface by dipping gold foil into a 1 mM solution of MPS solution in ethanol for 12 h, followed by rinsing in pure ethanol[71]. Negatively-charged groups have been placed onto a gold surface by immersing the surface in a 0.5 mM solution of 11-mercapto-undecanoic acid in acetonitrile for 30 min, followed by rinsing with acetonitrile and drying with a stream of warm air[76].

d. *Other Surfaces* PET has been used as a substrate for PMF films[18]. Hydrolysis in 1M NaOH for 16 min gives a surface containing carboxylic acid and alcohol functional groups and is

negatively charged at high pH. When a PAH solution is applied to the surface at high pH, amide linkages form between the carboxylate groups and some of the PAH amino groups. At lower pH, only electrostatic interactions occur. Single crystal silicon wafers are cleaned for 20 min at 60 ^{o}C in a solution containing 1 part 28% NH_4OH, 1 part 29% H_2O_2, 5 parts deionized water, followed by a deionized water rinse[77].

e. *Charging the Surface* Dipping silanized slides into a 1 N HCl acid solution gives them a net positive charge[38]. Freshly cleaved mica, silicon wafers, glass or quartz slides can be given a positive charge by covering with a layer of PEI. To charge the surface, the wafers are immersed in a PEI solution for 30 min[77]. A oriented crystal silicon wafer cleaned with Piranha solution gives a hydroxylated surface which forms positively charged monolayers when dipped into a 5% solution of PDDA [78]. It has been demonstrated that a plasma treatment yields a charged surface to adsorb polyelectrolyte layers[79].

2. Dip Time, Electrolyte Concentration and Ionic Strength

a. Dip Time A basic question associated with PMFs is determination of dip time for monolayer formation. Dip times yielding successful multilayer formation include 5-10 sec[78], 1 min[38], 5-10 min[74], 20 min[73, 80 , 81], 30 min[82 , 83] and 24 hours[84]. In all cases the citations have data showing a linear increase of thickness with number of dip cycles. Proper determination of dip time requires understanding of the mechanism of monolayer formation. Monolayer formation includes at least two steps: diffusion of the ion to the surface and binding to the surface. A calculation of film formation based on diffusion alone gives rates 100 times faster than observed rates[85]. Transition states similar to those seen in IPEC ion exchange studies(Section IIC) may form at the film/solution interface. QCM investigations of monolayer formation reveal first order kinetics with lifetimes of 5 min for proteins[81] and similar lifetimes for adsorption of dyes onto the multilayer surface. Figure 6 gives examples of deposition kinetics measured by QCM[73].

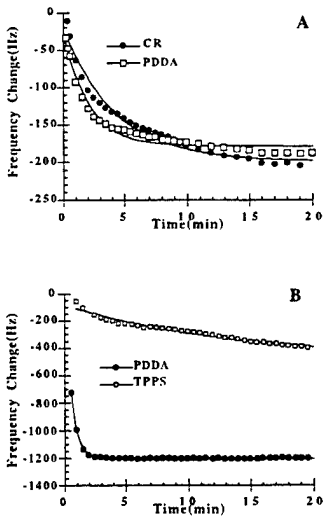

Figure 6. Adsorption kinetics monitored by QCM. A: CR/PDDA film. Adsorption half life was calculated to be CR: 2.5 min, PDDA: 1.5 min. B: TPPS/PDDA film. Adsorption half life was calculated to be TPPS: 6.3 min, PDDA: 0.39 min. Adapted with permission from reference [**72** 5]. Copyright 1997 American Chemical Society.

Figure 6A gives data for the CR/PDDA system. The polymeric PDDA has comparable adsorption kinetics to the dye CR, both saturating within 20 min. In contrast, the TPPS/PDDA system shows significant differences between dye and polymer behavior. In this case PDDA adsorbs completely within 5 min, while the porphyrin dye TPPS has not saturated after 20 min. Also, the adsorption half lifes for PDDA were different for a CR surface(1.5 min) *vs.* a TPPS surface(0.39 min). Because of the variation in kinetics, measurement of the rate of monolayer formation by the QCM technique will enable choice of dip times. As a rule of thumb, a 20 min dip time will usually give good results.

b. *Concentration* The relation between electrolyte concentration and film properties has not been explored in detail. Successful film formation has been demonstrated for electrolyte(monomer unit or individual molecule) concentrations ranging from 0.1 mM to 35 mM in deionized water[38, 73, 81, 86, 88-90]. A systematic measurement of the effect of electrolyte concentration suggests no strong electrolyte concentration dependence[73]. Table I shows QCM data for the CR/PDDA system[73]. There are no major differences in the amount of material deposited when either the CR or PDDA concentrations were varied. In general, good results can be obtained with the polyelectrolyte monomer concentrations being 0.01M, corresponding to a weight concentration of 1-3 mg/ml.

Table I

Frequency changes upon adsorption of CR or PDDA

[CR][a]	$-\Delta F$[b]	[PDDA][c]	$-\Delta F$[b]
1.0	84±7	19	42±12
10	73±12	1.9	43±23
1.0	77±13	1.9	60±15
0.1	74±9	1.9	50±15
0.01	78±10	1.9	46±8

[a]Reprinted in part with permission from reference [73]. Copyright 1996 American Chemical Society.
[b]Dye concentration(mM) in water. Dip time was 20 min with water washing between adsorption steps.
[c]Frequency decrease(Hz) per dye or polycation adsorption step measured from QCM
[d]Polycation concentration(mM). Dip time was 20 min with water washing between adsorption steps.

c. *Rinsing and Drying* A rinsing step is usually included in published film preparation procedures. To ensure linear film buildup, a precursor film $(PSS/PAH)_2$ should be placed onto the substrate surface. A commercially available automated slide stainer has been used to prepare PMFs[91]. Hoogeveen[22] describes the effect of rinsing on the kinetics of monolayer formation. Film deposition is monitored by measuring reflectance. During rinsing, no major changes in film reflectance were observed. During the subsequent adsorption step, significantly more material adsorbs onto the film surface. Rinsing appears to cause changes in film morphology which facilitate adsorption of a new layer. A two minute rinse will usually give good results.

Drying the film with a nitrogen stream is necessary when analytical measurements will be performed. However, drying may affect film morphology. The effect of drying-induced manipulation of the film surface at regular intervals has been investigated in $(PSS/PAH)_n$ films[92]. Instead of keeping the film wet throughout all deposition cycles, the films were dried at regular intervals during alternating deposition of a PSS polyanion or PAH polycation. For example, when the films were dried after every 6th layer, X-Ray reflectance measurements showed the appearance of higher order Bragg peaks, suggesting reorganization of film structure to form unit cells larger than the bilayer thickness[92]. Drying procedure effects on thickness were shown in $(Pre\text{-}PPV/PVS)_{12}$ films[93]. When the films were dried after four adsorption cycles and there was no salt present in the dipping solution, the thickness per bilayer was 47Å.

The bilayer thickness increased to 90Å when the films were dried after each adeosption cycle. The difference became negligible under high salt conditions.

d. *Ionic Strength* Ionic strength has been found to have a major effect on deposition kinetics and the amount of material deposited onto the surface. The presence of counterions shields the electrolyte charges and increases the rate of adsorption[14]. A detailed investigation of ionic strength effects on colloidal silica particle adsorption has been performed[94]. At ionic strengths below 200 mM, the mass uptake per layer was directly proportional to ionic strength. At higher ionic strength, the mass uptake increased with the square root of ionic strength. An investigation of $(SiO_2/PDDA)_n$ films revealed a strong dependence of ionic strength on mass uptake[95]. When the ionic strength was 0M, the film mass was 8.1 μg, increasing the ionic strength to 0.25M caused the film mass to increase to 47 μg.

B. Methods for Characterizing Polyion Multilayer Films

1. X-ray small-angle reflectometry method

A powerful method for measuring film thickness is small angle X-ray reflectance(SAXR)[96]. X-ray reflection from a uniform film on a substrate having a thickness L exhibits interference between waves reflected at the air/film interface. An example of X-ray reflectivity data is shown in Fig. 7.

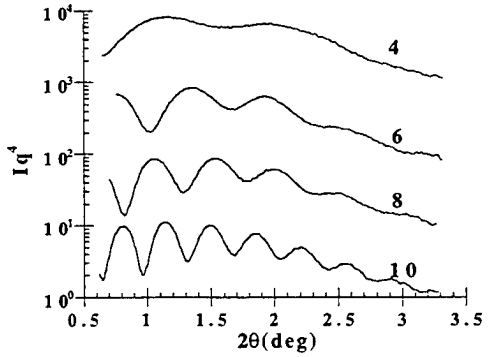

Figure 7. X-Ray reflectivity data for PSS/PAH adsorbed on optical waveguides precoated with boladication. Data shown are for 4, 6, 8 and 10 monolayers(2,3,4 and 5 bilayers). Figure adapted with permission from J. J. Ramsden, Y. M. Lvov and G. Decher *Thin Solid Films* **254**, 246, (1995), Copyright 1995 with permission from Elsevier Science, The Boulevard, Langford Lane, Kidlington 0X5 1GB, UK.

A plot of reflectance *vs.* incident angle yields Kiessig fringes whose minima or maxima show a regular spacing $\Delta\theta$ and film thickness can be estimated from

$$L = \frac{\lambda}{2\Delta\theta} \tag{7}$$

where λ is the X-ray wavelength. Electron density and film roughness can be measured by fitting experimental data to a suitable theoretical model.

2. Optical Spectroscopy

a. *UV/Vis Spectroscopy* If the PMF has a chromophore, UV/Vis spectroscopy. UV/Vis spectra of PMFs show a linear buildup of absorbance[9, 38, 73, 86, 90]. Kinetics of film deposition can be monitored by UV/Vis. By monitoring the absorbance at 420 nm, the kinetics of deposition of a single monolayer of PTAA onto a PAH layer has been monitored[97]. Multilayers of positively and negatively charged colloidal particles like silica and alumina exhibit interference colors which exhibit maxima and minima in their reflection bands from which thickness can be determined[69].

b. *Ellipsometry* Ellipsometry is another technique for measuring film thickness[98]. Spectroscopic ellipsometry involves measurement of the phase and amplitude change upon reflection of s or p polarized light. The basic equation of ellipsometry is

$$\rho = \tan(\Psi)e^{i\Delta} \tag{8}$$

where ρ is the ratio of complex reflectances between s or p polarized light, Δ represents the relative phase shift between the s and p components and Ψ represents the change in intensity. Δ and Ψ are functions of film thickness and refractive index. At any wavelength two equations(Δ and Ψ) are a function of three variables: film thickness(d), the real(n) and imaginary(k) index components. When k = 0, n and d can be solved for a given film model. When k 0, two variables can be obtained by fixing the third. An example of refractive indices obtained from ellipsometric data is given in Fig. 8.

The data show calculated n and k for a series of $(PLL/Cu\text{-}PTSA)_n$ films. By fixing d, n and k were calculated. The trends in n and k reflected changes in film roughness and homogeneity. The calculated imaginary component k became independent of thickness with optical density greater than one[99].

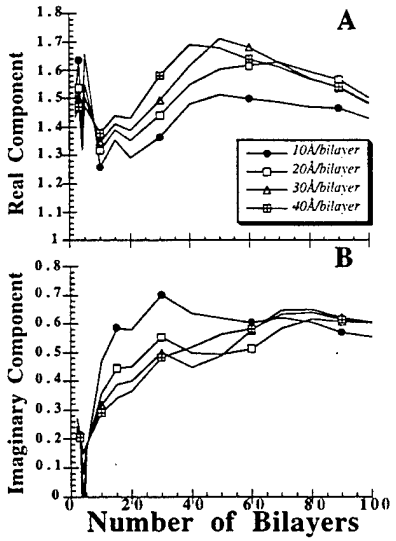

Figure 8. Real(A) and imaginary(B) refreactive index components calculated from ellipsometric data for (PLL/Cu-PTSA)$_n$ films. Reprinted with permission from reference [38]. Copyright 1995 American Chemical Society.

It was then possible to use a simple expression for film thickness obtained from the absorbance(A) and k[38].

$$L = \frac{2.303A\lambda}{4\pi k} \tag{9}$$

With this approach, film thickness can be measured. Real time ellipsometry has also been used to monitor deposition kinetics of the amphiphilic PAM onto a self-assembled mercaptoalkanoic acid monolayer on gold[100].

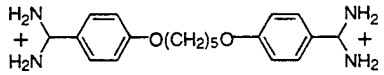

PAM

VII

c. *Reflectance* Hoogeveen[22] describes reflectance measurements of PMFs. For small reflectances, the reflectometer signal is given by

$$\Gamma = \frac{1}{A_S}\frac{\Delta S}{S_O} \tag{10}$$

where A_S is the sensitivity factor proportional to the refractive index increment of the polymer.

Caruso used reflectance measurements on gold substrate PMFs as gold is highly absorbing[75]. His reflectance measurements were referenced to the substrate, so reflectance data could be converted to absorbance using

$$A = -\log(\frac{R}{R_0}) \tag{11}$$

where A is the absorbance, R is the reflectance from the gold plate with adsorbed multilayer and R_0 is the reflectance from the gold plate. PMFs have been characterized by total internal reflection fluorescence(TIRF) spectroscopy[36, 101]. The technique requires a fluorescent species to be present in the film. An argon-ion laser beam couples into the glass substrate through glass prisms. The evanescent field at the substrate surface excites the fluorescent dye in the film. The fluorescent light is collected by an optical system and analyzed by an optical multichannel analyzer. In order to investigate different experimental conditions, the substrate serves as the top of a flow cell flushed by a pump.

d. *Surface plasmon resonance* Surface plasmon resonance spectroscopy has been used to measure PMF thickness and deposition kinetics. The technique involves production of a surface plasmon, a transverse magnetic electromagnetic wave traveling along the interface between two media[102]. The experimental apparatus consists of a prism on which a 70 nm gold film has been deposited. The surface plasmon mode can be excited by the evanescent field arising from total internal reflection inside the prism. By measuring the intensity of the reflected light as a function of incident angle into the prism, a resonance angle can be found giving maximal production of the evanescent field. Deposition of a thin film onto the gold layer causes the resonance angle to vary. The reflectivities can be fit to the Fresnel equations for the system, from which refractive index and film thickness can be obtained. Examples of surface plasmon resonance measurements on PMF systems include polymer[21, 75, 103], nanoparticle[8] and protein systems[20]. IR spectroscopy has been used to monitor material deposition[34]. Albumin, adsorbed onto a germanium crystal, can be monitored with infrared multiple internal reflection spectroscopy. Deposition kinetics have been measured from the albumin absorbance at 1, 549 cm^{-1}. Deposition of heparin onto an albumin monolayer has been monitored from the absorbance at 1, 030 cm^{-1}.

3. Atomic Force Microscopy/Scanning Tunnelling Microscopy

Atomic force microscopy(AFM) and scanning tunneling microscopy(STM) are kindred microscopy techniques that give resolution down to the atomic level[104-106]. STM measures the electrical tunneling current that flows between two conductors(the STM tip and the analyzed

surface) separated by distances on the order of Ångstroms. Factors influencing the current include the distance between the two conductors and their electron band structure. The technique has been particularly succesful in imaging molecules containing aromatic groups. The more popular AFM technique does not require electrically conducting surfaces but rather measures forces between the scanning tip and the surface including electrostatic, magnetic and van der Waals forces. Another variant on these techniques is friction force microscopy[104], where both horizontal and vertical forces between the tip and the surface are investigated. By modifying the AFM tip with hydrophobic or polar groups, a direct probe of specific intermolecular forces has been demonstrated[107]. Although these techniques enable imaging of molecular and atomic scale objects, the microscopy saying "Believing is seeing" applies. Sources of artifacts include room vibrations, electrical noise, confusing step edges in the substrate or the substrate itself with adsorbed molecules and monolayers and scratches on the surface formed by the AFM tip. As well as images, AFM has been used to measure film roughness defined as the RMS difference between peak and valley height. A recent variation on the technique is chemical force microscopy. By chemically modifying the cantilever tip with specific groups(hydrogen bond donors, hydrophobic groups, etc.), it is possible to image a surface in terms of specific intermolecular forces.

AFM has been used to characterize PMFs and give insight into the mechanism of film formation. Multilayers composed of a cationic polyelectrolyte and individual sheets of the mineral hectorite have been prepared[78]. Individual hectorite sheets 25 to 30 nm in dimension are imaged by AFM. A common observation with PMFs is increased surface roughness and poor deposition of material with less than five monolayers. Direct AFM observations of PSS monolayers showed non-uniform deposition at the earliest stages[108]. At short deposition times(1 min), the charged macromolecules adsorbed onto surface defects, forming islands and retaining their coil conformation. At longer deposition times(10 min), homogenous monolayers composed of flattened polymer chains formed. AFM has been used to study the adsorption of charged latex particles on mica[109]. Because latex particles are large and easy to image, AFM was a useful tool to probe the mechanism of monolayer formation in PMFs. Surface coverage, determined by analysis of AFM images, was measured as a function of adsorption time and ionic strength. From analysis of the images, the initial kinetics are diffusion limited converting to random sequential adsorption at long times. For each ionic strength, surface coverage rose rapidly during the early stages of adsorption, then leveled off. The total surface coverage increased dramatically with increasing ionic strength. At low ionic strength, long-range repulsions between latex particles limited the extent of adsorption. At higher ionic strength, interparticle repulsions decreased due to double layer screening. *In situ* images of adsorbed

layers differed from those of dried samples, showing rearrangement of the particle packing upon evaporation.

4: Quartz Microbalance

The quartz crystal microbalance(QCM) technique allows for real-time monitoring of rate and amount of monolayer deposition during PMF monolayer formation. The QCM is a piezoelectric device capable of measuring mass changes on the order of nanograms. The Sauerbrey equation describes changes in the resonant frequency of a quartz crystal with the change of mass of material loaded onto the crystal[110].

$$\Delta f = \frac{-2\Delta m f_0^2}{(\rho_0 \mu_0)^{1/2} A} \qquad (12)$$

where f_0 is the fundamental frequency, ρ_0 is the density, μ_0 is the shear modulus of the unloaded quartz crystal. When a mass Δm deposits upon a crystal of area A, the resonant frequency decreases by Δf. For a 9 MHz quartz resonator, the relationship between adsorbed mass(g) and frequency shift(Hz) is

$$\Delta F = -1.83 \times 10^8 \frac{M}{A} \qquad (13)$$

For a resonator area of 0.16 cm^2, a 1 Hz frequency change corresponds to 0.9 ng mass increase. The technique can be used measurement of the mass of a dried film. After drying the sample in a nitrogen stream, the resonance frequency can be measured and the Sauerbrey equation used to calculate the adsorbed mass.

Figure 9 shows a plot of frequency decrease as a function of the number of adsorption steps for $(CR/PDDA)_n$ and $(CR/PEI)_n$. In $(CR/PDDA)_n$(Fig. 9A), the frequency decrease represents monotonic adsorption of dye and polymer. In the second case, $(CR/PEI)_n$(Fig. 9B), the frequency increases in the presence of PEI, showing partial dye desorption.

The QCM technique can also be used to measure film thickness[81]. For example, in $(GOx/PEI)_n$ films, a plot of Δf *vs.* number of adsorption cycles had a linear decrease in frequency past five films. The frequency change per cycle had two components: -2,150 Hz for GOx and -50 Hz for PEI. By making assumptions about film density, a "rule of thumb" equation of thickness on both sides of a 0.16 cm^2 electrode is

$$L(\text{Å}) \cong -0.16\Delta f(\text{Hz}) \qquad (14)$$

giving a bilayer thickness of 350Å. The technique can also be used for adsorption kinetics measurements. By placing one side of the resonator in permanent contact with the solution, real time measurements of the resonance frequency can be obtained. To prevent a short circuit, the upper contact wire is insulated from the solution by convering with silicone paint. Alternatively, there are commercially available beakers with resonators mounted so that only one side is exposed to the sulution. An example of QCM kinetics data is given above(Fig. 6).

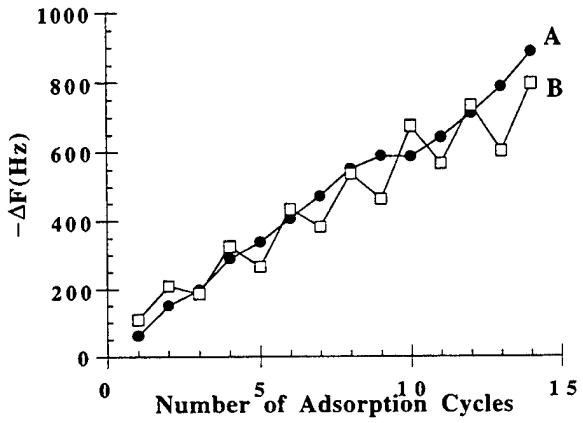

Figure 9. Frequency decrease(-ΔF) measured by QCM upon dye-polyion film adsorption. A: Odd numbered steps represent adsorption of 1mM CR. Even numbered steps represent adsorption of 1.9 mM (in monomr) PDDA. B: Odd numbered steps represent adsorption/desorption of 10 mM CR. Even numbered steps represent adsorption of 35 mM(in monomer) PEI. Adapted with permission from reference [73]. Copyright 1997 American Chemical Society.

5. Contact Angle Measurements

Contact angle measurements have been used to characterize PMFs. Unless it wets the surface, a liquid placed on a solid will form a drop having a contact angle between the liquid and solid phases. The contact angle is given by Young's equation[111].

$$\gamma_{LV}\cos\theta = \gamma_{SV} - \gamma_{SL} \qquad (15)$$

where θ is the contact angle and γ_{LV}, γ_{SV} and γ_{SL} are the surface energies for the liquid-vapor, surface-vapor and surface-liquid interfaces, respectively. When $\theta = 0^{o}$, the liquid wets the surface. When $\theta = 180^{o}$, a spherical droplet forms on the surface. Tables of contact angles for various surfaces have been prepared[111]. Hydrophobic surfaces have contact angles around

110°, while hydrophilic surfaces approach 0°. A methods for measurement of the contact angle have been described by Murray[112] and Adamson[111]. For accurate measurements, Murray recommends making multiple measurements on the same drop and having awareness of the effect of surface roughness and heterogeneity on the contact angle. The technique involves measurement of the shape of a liquid drop deposited onto a surface or the contact angle of the meniscus during dipping or withdrawal from the liquid. Liu[113] gives advancing water contact angle measurements of a TiO_2/PSS multilayer(Fig. 10).

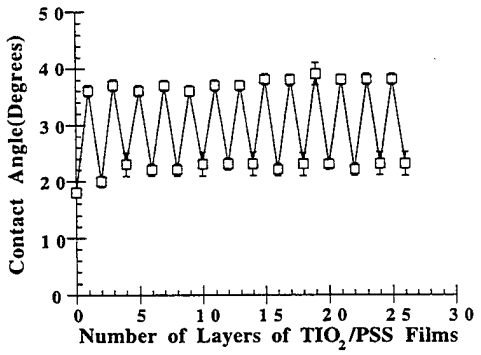

Figure 10. Advancing contact angles of TiO_2/PSS multilayer films as a function of the number of deposited monolayers. Adapted with permission from reference [113]. Copyright 1997 American Chemical Society.

Glass treated with *N*-2-(2-aminoethyl)-3-aminopropyltrimethoxysilane gave a contact angle of 18°. Anionic PSS adsorbing on this surface increased the contact angle to 37°. The increased contact angle resulted from adsorption of PSS with polar sulfate groups interacting with the positively charged surface and the nonpolar hydrocarbon chains oriented toward the surface. When cationic TiO_2 adsorbed onto a PSS surface, the contact angle decreased to 22°. The lower contact angle reflects the hydrophilic nature of cationic TiO_2. The contact angle oscillated between these two values as the multilayer built up. Chen describes similar oscillations in a PSS/PAH multilayer prepared on a PET substrate[18]. These results illustrate the utility of contact angle measurements for characterizing PMF films, as the film surface energy significantly changes with adsorption of different materials.

6. X-ray photoelectron spectroscopy

X-ray photoelectron spectroscopy(XPS) has been used to measure the element composition of the surface of PMF films[114]. A thin film is irradiated with soft X-rays and

photoelectrons are emitted. The photoelectrons are collected by a lens system and an analyzer counts the number of electrons at a given kinetic energy. The data are presented as a plot of counts per second *vs.* binding energy, given by

$$B.E. = h\nu - K.E. - \phi \tag{16}$$

where $h\nu$ is the X-ray energy, ϕ is the sample work function, K.E. is the kinetic energy of the photoelectron and B.E. is the binding energy. The binding energies derive from the atomic core 1s level from which the photoelectron was emitted and can therefore be used for analysis of the elemental composition of the surface. The surface sensitivity of XPS results from the distance an electron of a certain kinetic energy can travel through a material before undergoing an inelastic collision. The attenuation of photoelectron intensity as a function of sampling depth is given by

$$N = N_0 e^{-t/\lambda\cos\theta} \tag{17}$$

where N_0 is the number of photoelectrons that originate at depth t, N is the number of photoelectrons that have not inelastically scattered, λ is the mean free path of the electron and θ is the takeoff angle. The sampling depth, that depth which gives 95% of the signal intensity, is $3\lambda\cos\theta$. Munro lists mean free paths ranging from 7-15Å. By varying θ, different depths of the sample can be probed. Delcorte gives an extensive study of PMF films, containing correlations of XPS data with ToF-SIMS, SAXR and AFM[13]. An example of XPS data from a PMF film is given in Fig. 11.

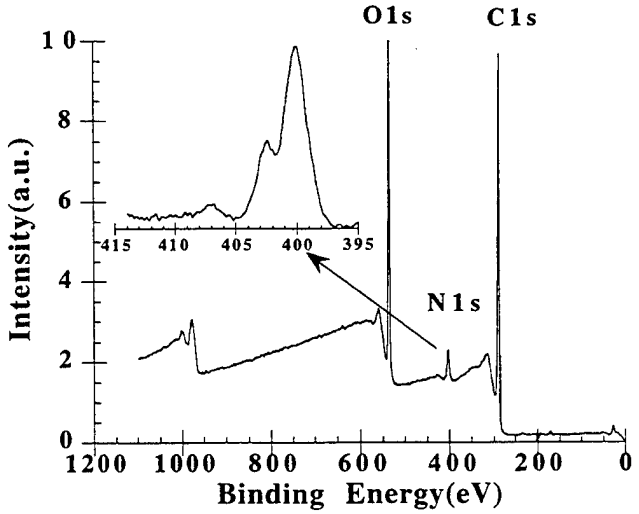

Figure 11. Example of XPS data. Data collected from chitosan + (sulfonated C_{60}/tetrapyridinium porphyrin)$_{10}$ film. The inset gives high resolution data collected in the vicinity of 400 eV. Data are courtesy of Dr. Hao Jiang, Anteon Corporation, Dayton, OH.

The XPS spectrum was obtained from a (sulfonated C_{60}/TMPyP)$_{10}$ film that had been placed onto a chitosan-treated glass slide. High resolution XPS data (inset to Fig. 11) showed fine structure associated with nitogen. The satellite peak at 407 eV resulted from charge transfer interactions between sulfonated C_{60} and the porphyrin.

C. Polymer/Polymer Films

1. PSS/PAH

PMFs composed of PSS/PAH bilayers have been investigated in detail and serve as a model system. An early study demonstrated the formation of thin films composed of up to 50 PSS/PAH bilayers[80]. The absorbance and film thickness determined by SAXR increased linearly. Thin films containing PAH/PSS bilayers have been successfully grown on gold surfaces[75]. Regular film buildup was observed after placing two PAH/PSS precursor bilayers onto the gold surface. PAH/PSS multilayers have also been prepared on a PET substrate[18].

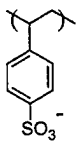

PSS

PAH

VIII-IX

a. *Structure and Composition* The structure of films composed of PSS/PAH bilayers have been probed by X-Ray scattering, neutron reflectivity and optical waveguiding experiments. To prove that multilayer organization exists in PMFs, films having the composition (PSS/PAH + PAZO/PAH)$_n$ were made[92].

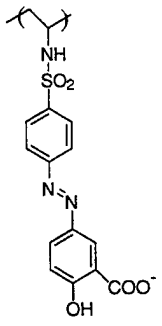

PAZO

X

A Bragg peak in X-ray reflectivity gave a spacing of 93.4 Å corresponding to the four layer repeat unit.

Combined neutron reflectivity and SAXR measurements were performed on partially perdeuterated PSS/PAH films[83] The film [PSS-h_7/PAH + PSS-h_7/PAH + PSS-d_7/PAH]$_8$ had one perdeuterated layer every six layers. The layers were deposited from high ionic strength solutions. A schematic of a PSS/PAH bilayer is depicted in Fig. 12.

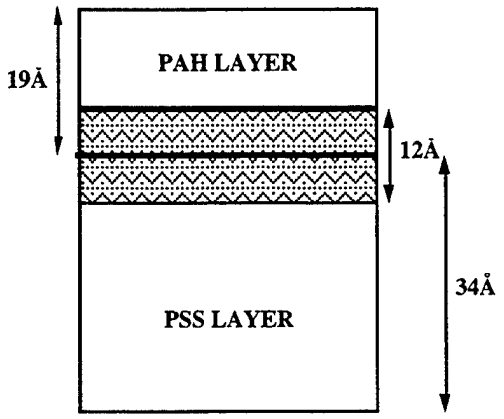

Figure 12. Schematic of PAH/PSS bilayer using data from reference [83]. The bilayer is composed of a PSS layer, a PAH layer and an 12Å thickness interdigitation region.

The authors analyzed the film in terms of its constituents: polyelectrolyte, water and counterions. Film thickness measured by SAXR and neutron reflection agree, giving a bilayer thickness of ~50Å. The large monolayer/monolayer roughness(19Å) reflected considerable chain/chain interdigitation. Film composition data suggested a high water(4 water molecules per monomeric PSS unit) and estimated counterion content(0.5-0.8 anions/cations per polyelectrolyte repeat unit), as well as a non-stoichiometric N_{PAH}/N_{PSS} = 1.5. The monomer ratio agreed with XPS data obtained from PSS/PAH multilayers adsorbed on PET. In that study the ratio of nitrogen to sulfur ranged from 1.3-2[18]. Evidence for the presence of water in PMF films was obtained from a thermal stability study of PSS/PAH films[39]. A $(PSS/PAH)_{20}$ was annealed at 190°C for 3 h. Comparison of FTIR spectra before and after annealing showed a decrease in absorbance at 3,450 cm^{-1}, corresponding to water loss.

The structure of a PSS/PAH multilayer has been probed through the use of optical waveguide experiments[85]. The PSS dipping solution contained 0.5 M $MnCl_2$, while the PAH dipping solution contained 2M NaBr. The thin film had three refractive index tensor components: two equal n_o components parallel to the substrate and one component n_e perpendicular to the substrate. As the number of layers increased, n_o decreased and n_e increases,

giving a positive birefrengence $n_e - n_o$. The birefringence increased from 0.036 in a two bilayer film to 0.081 in a 5 bilayer film. The birefringence data suggested the polymers tended to lay parallel to the substrate surface when there were a few bilayers and formed polymer loops and chains oriented perpendicular to the substrate where there were more bilayers.

b. *Ionic Strength Effects* As well as polymer concentration, dip time and substrate properties, dipping solution ionic strength has a significant effect on film thickness. Table II lists the results of several studies focusing on ionic strength effects.

Table II

The effect of ionic strength on bilayer thickness in PSS/PAH multilayers

PAH solution[a]	PSS solution[b]	Bilayer Thickness(Å)	Reference
0.0	0.0	10.7	[9]
0.0	0.5	14.0	[9]
0.0	1.0	17.2	[9]
0.0	1.5	19.4	[9]
0.0	2.0	24.0	[9]
2.0	2.0&1.5	51.0[c]	[9, 79, 80, 83, 85, 92, 169, 170]
0	3.0	100	[75]

[a]Ionic strength of low molecular weight electrolyte(NaCl or NaBr) added to PAH solution.

[b]Ionic strength of low molecular weight electolyte(NaCl, NaBr or $MnCl_2$) added to PSS solution.

[c]Bilayer thickness is average of estimates given in the references.

By changing the ionic strength of the anionic electrolyte solution while keeping the cationic electrolyte solution at low ionic strength, bilayer thickness could be varied by a factor of 2[9, 115]. With both the PAH and PSS solutions at high ionic strength, the bilayer thickness increased by another factor of 2[9] (and other references cited in Table II). When the films prepared from high ionic solutions were placed in water, the salts did not leave the film. Instead the films swelled 6-10% over 15 days. The increased thickness remained upon drying[9]. A PSS/PAH film prepared from low ionic strength solutions showed similar swelling/drying behavior but was four times thinner.

The salt effect resulted from ionic strength effects on polyelectrolyte conformation. Early investigations of polyelectrolyte adsorption on surfaces revealed the polymer had a "flat" conformation on a highly charged surface in the presence of a low ionic strength medium[116].

With increased ionic strength, intersegmental electrostatic repulsion was suppressed and the polyelectrolyte chain assumed an extended conformation(Fig. 13).

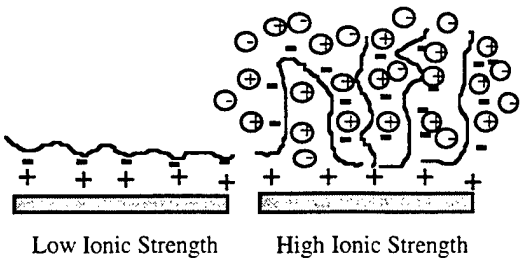

Figure 13. Schematic of polymer monolayer under conditions of low and high ionic strength. High ionic strength lessens electrostatic repulsion, promoting formation of loops, trains and tails.

Advancing contact angle measurements provided another probe of the effect of dipping solution ionic strength on film properties[18]. In a series of PSS/PAH multilayers having PAH as the outermost layers, the advancing contact angle was 70^{o} when 1.0M $MnCl_2$ was in both dipping solutions. When $MnCl_2$ was only in the PSS solution, the angle decreased to 60^{o}. When no $MnCl_2$ was used, the angle decreased to 46^{o}. When the PSS layer was the outermost layer, the ionic strength effect was smaller, with the contact angle being 45^{o} in both experiments using $MnCl_2$, increasing to 53^{o} with no $MnCl_2$ present. The PSS layer tended to be more wettable than the PAH layer, possibly reflecting the tendency of the sulfate groups orienting near the surface facing the dipping solution and the aromatic rings orienting away from the surface. When PAH was on the surface, the films became less wettable with increasing ionic strength of the dipping solution. To a lesser degree the opposite trend occurred with films having PSS on the surface. The trends reflect dipping solution ionic strength effects on the relative proportion of film surface hydrophobic and hydrophilic groups.

Increasing ionic strength also caused reversible thickness changes in previously prepared PMFs[77]. A series of PSS/PAH multilayers were prepared and immersed in varying ionic strength salt solutions. After the salt solution was removed, film thickness was measured by SAXR. Film thickness changes up to 18% were complete after 1-2h immersion time. By immersing the films into deionized water, the film swelling could be reversed within experimental error. Also, the films became smoother after several cycles of dipping into salt solutions and deionized water. Measurement of film thickness changes as a function of salt concentration revealed a small range of salt concentrations (0.02 - 0.1 M) where swelling occured. When the concentration was below 0.02M, no swelling occured. Also, no further swelling occured with the concentration greater than 0.1M. Changes in the proportion of loops, trains, tails, intralayer entanglements, the width of the polyanion/polycation interface and salt bridges could contribute to the observed swelling changes, although the exact structural changes

are unknown.

c. *Electrostatic Properties* The electrostatic properties of a PSS/PAH multilayer have been probed through the use of a pH-sensitive fluorescent dye[36]. PAH was derivatized with fluorescein isothiocyanate to form FITC-PAH. Initially, a 140Å precursor film containing layers of PEI, PSS and PAH was placed onto the substrate.

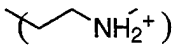

PEI

XI

After the last PSS layer of the precursor film, a monolayer of FITC-PAH was placed onto the film. Then, varying numbers of PSS and PAH layers were placed onto the FITC-PAH layer.

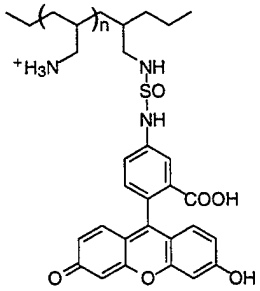

FITC-PAH

XII

The dye fluorescence was measured by the TIRF technique under conditions of varying external pH. Shifts in the pH titration curve monitored by fluorescence gave information about the proton concentration gradient in the multilayer.

The authors considered three parameters: film thickness, charge on the film surface and ion concentration of the buffer solution. The nature of the group on the surface of the film had a significant effect on the pK_a of the FITC-PAH. The pK_a of FITC-PAH in solution was 4.6. For all films with PAH as the outermost layer, the pK_a was 5.9. In contrast, films with PSS on the surface had a pK_a of 7.5 for the thinnest films, decreasing to 5.8 for the film $(PSS/PAH)_8$ + PSS. The pH effect on fluorescence intensity decreased with increasing film thickness, with no effect beyond 100 Å thickness above the FITC-PAH layer. When in the presence of divalent cations, the portion of the titration curve that could be measured of films having a PSS surface layer shifted to a lower pK_a. The divalent cations neutralized the sulfonate charge, thereby decreasing

proton affinity. In the presence of buffered high salt concentration, films having a PSS surface layer had increased fluoresence intensity, while films having a PAH surface layer showed decreased intensity. The results for films with a PAH surface were not reversible, reflecting salt-induced morphology changes. The salt effect was negligible in thick films. The ionic strength effect on fluorescence intensity was attributed to ionic strength effects on pK_a. When PAH was on the surface, the pK_a increased, while it decreased with PSS on the surface. The Gouy-Chapman-Stern model was used to describe the ion distribution inside the film. The electrical potential decayed exponentially with a decay length being a function of surface charge and ionic strength.

A more recent study uses similar strategies to measure transport through a PMF[101]. A series of fluorescent films containing a FITC-PAH layer was prepared as above. A rhodamine solution was added to the outer aqueous phase and diffusion of the dye into the multilayer was measured by energy transfer between the dyes that quenched FITC-PAH fluorescence. A depth-dependent diffusion coefficient of 10^{-15} cm^2 s^{-1} was measured for the rhodamine dye. The smaller paramagnetic quencher 2,2,6,6-tetramethyl-4-piperidinol-1-oxide had a diffusion coefficient at least two orders of magnitude larger.

d. *Gas Transport* Stroeve describes the gas-permeation properties of PSS/PAH multilayers[117]. Multilayers were placed onto and silicone membranes and gas permeability measured. A polyion film adsorbed onto a silicone membrane gives significantly reduced gas permeability compared to an untreated membrane. Because of incompatibilities in mechanical properties, microcracks appear in the multilayers, forming leaks and increasing gas permeability. The polyion coated membrane gives increased CO_2/N_2 selectivity, so the multilayer films have a possible application as a gas separation membrane. In a related study, Lavasalmi prepared PSS/PAH films on a surface oxidized poly(4-methyl-1-pentene) substrate with the goal of developing an asymmetric gas separation membrane[118]. The PSS/PAH multilayer has 18,000 times lower gas permeability to N_2 than the substrate alone.

2. Other Polymer/Polymer Systems

Thin films composed of bilayers PVS/PAH have been prepared[88].

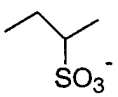

PVS

XIII

Unlike PSS/PAH films described above, film buildup could not be followed spectrophotometrically but rather from SAXR. Similar to the systems described above, increased ionic strength caused the bilayer thickness to increase from 13 Å to 34Å. Film thickness of a 24 bilayer PVS/PAH film was measured as a function of temperature. From room temperature to 50 °C the film thickness remained constant. From 60 to 120 °C, the film thickness decreased 6%. The film thickness remained constant to 150 °C. When the film cooled, the high temperature thickness remained constant. After 2 weeks, the film thickness nearly returned to its initial value. A likely explanation for the thickness changes is the removal/addition of water.

The SA technique has been extensively used to prepare multilayers of conjugated polymers, thereby providing a means to assemble thin films with novel electrical and optical properties. PMFs containing the conjugated polymers SPAn, polyimide precursor and PTAA have been investigated for potential electro-optic applications[97, 119].

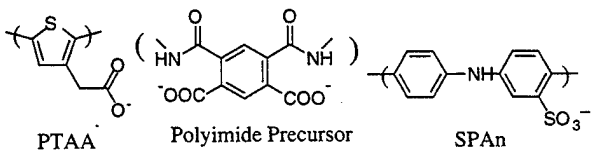

XIV-XVI

For both SPAn/PAH and PTAA/PAH films, the amount deposited is directly proportional to the number of bilayers. During short deposition times, adsorption kinetics followed a diffusion-controlled adsorption process, slowing thereafter. In the pH range 4.8 - 6.4, adsorption of PTAA onto a charged surface was dependent upon pH. The equilibrium amount of PTAA adsorbed increases with increasing pH. The pK_a of PTAA was near 4.6, so protonation of ionized acetate groups enhanced adsorption by decreasing electrostatic repulsion. In the pH range 2.0-4.0, films containing SPAn showed less dependence of deposition on pH with the amount adsorbed increasing with decreasing pH. In this case, NH groups in SPAn were protonated, decreasing the net charge and electrostatic repulsion. The more complex film $(SPAn/PAH/PTAA/PAH)_{20}$ has also been prepared. The UV/Vis data showed linear increase in the amount of both polymers deposited with increasing number of bilayers.

Light-emitting diodes have been prepared by the SA technique[120]. Multilayers containing the negatively charged polymers PSS or PMA and the positively charged *p*-phenylene vinylene precursor(pre-PPV) were prepared using a programmable slide stainer(HMS programmable slide stainer, Zeiss Inc.).

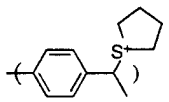

pre-PPV

XVII

After the slides dried overnight under a vacuum, pre-PPV converted to PPV by heating at 210 ^{o}C under vacuum for 11 hours, followed by 4 hour cooling period. Following film preparation, an Al layer was depositied by thermal evaporation onto the film. The intensity of both the absorption spectra and photoluminescence spectra of the films are directly proportional to the number of bilayers. Another example consists of SPAn/pre-PPV multilayers that have been thermally converted into electroluminescent films[121] and PVS/pre-PPV[93].

More complex heterostructures have been fabricated as light-emitting diodes[122]. Onitsuka fabricated a series of PPV-containing thin films and measured the voltage/current/light intensity relationship. He found the nature of the anion layers had a significant effect on the electrical properties of the films. He compared the weak carboxylic acid functional group of PMA with the strong sulfonic acid group of PSS.

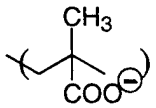

PMA

XVIII

Devices based on PMA/PPV had consistently higher light levels than PSS/PPV, possibly due to *p*-type doping taking place between the acidic sulfonic PSS groups and PPV's conjugated backbone, creating polarons and bipolarons which quenched luminescence. However, SPS/PPV films efficiently transported holes into PMA/PPV bilayers. To use this property advantageously, a heterostructure of the type ITO + $(PSS/PPV)_5$ + $(PMA/PPV)_{15}$ + Al was made. Compared to devices fabricated with only PMA/PPV bilayers, an order of magnitude luminescence increase occurred. Film performance was a strong function of the nature of the heterostructure. For example, they prepared a series of heterstructure devices ITO + $(PMA/PPV)_{20}$ + $(PSS/PPV)_n$ + Al, with n varying from 1 to 20. A single PSS/PPV bilayer dramatically decreased the output of the device. When n=5, the device had negligible output. Opposite performance was observed in the devices ITO + $(PSS/PPV)_n$ + $(PMA/PPV)_{20}$ + Al. Up to n=10, the luminescence intensity increased with the number of PSS/PPV bilayers. This behavior resulted from the ability of the

PSS/PPV bilayer to increase the electron injection barrier at the Al electrode or trap electrons injected from this electrode. Both behaviors can be controlled by preparing a suitable heterostructure. A related system was prepared from multilayers consisting of Bu-PHPyV/PSS bilayers[29].

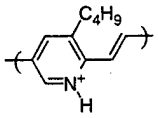

Bu-PHPyV

XIX

A multilayer assembly of redox polyelectrolytes has been prepared[71]. CV of multilayers having the composition $(PBV/PSS)_n$ showed linear increase in peak current with n.

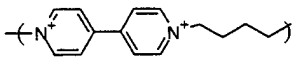

PBV

XX

The result suggested that all electroactive material in the film underwent oxidation and reduction, thus requiring an electron-hopping mechanism between bilayers. A strong influence of distance between PBV layers and the electrode was observed. A series of multilayers Au + MPS + $(PAH/PSS)_n$ + PBV/PSS was prepared. For n=1-3, the CV was similar to the results described above, except the slower electron transfer caused a greater cathodic/anodic peak separation. When n=4 or greater, no current was detected. Extensive interpenetration between layers was shown by variable angle XPS which revealed a 1:1 stoichiometry between charges in the multilayers. No salt ions were detected.

Tsukruk describes multilayer films prepared from dendrimers[123]. He used PAMAM dendrimers with surface amine groups from generations 4, 6 and 10 as the positively charged polymers and dendrimers with carboxylate surface groups from generations 3.5, 5.5 and 9.5. All even generations formed homogeneous, stable monolayers on a silicon surface. Monolayer thickness was much smaller than the diameter of hypothetical spherical dendrimers, implying compression of the dendrimers into oblate spheroids with axial ratios ranging from 1:3 to 1:6. Multilayers with the composition $(G_n/G_{n-0.5})$ were successfully prepared with thickness ranging from 1.8 to 5.6 nm/monlayer with 100-fold variation in dendrimer molecular weight.

Nonlinear optical effects have been demonstrated in PMF films[124]. He prepared films

having an azobenzene-containing polyanion PAZO. $(PEI/PSS)_2$ + $(PDDA/PAZO)_n$ multilayers showed generation of second harmonic radiation at 532 nm upon irradiation at 1064 nm.

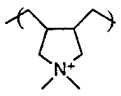

PDDA

XXI

Measurement of the angular dependence of second harmonic intensity while rotating the film gave Maker fringes, behavior expected for a noncentrosymmetric film(Fig. 14).

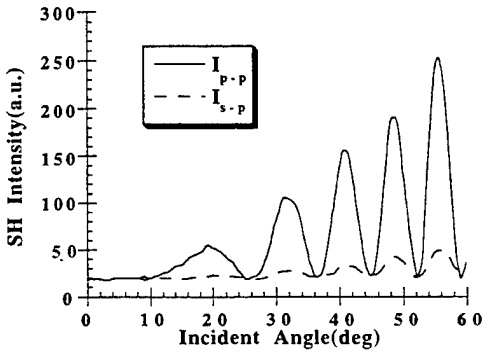

Figure 14. Example of Maker fringes in $(PDDA/PAZO)_4$ film. Figure adapted with permission from Y. Lvov, S. Yamada and T. Kunitake *Thin Solid Films* **300**, 107, (1997), Copyright 1997 with permission from Elsevier Science, The Boulevard, Langford Lane, Kidlington 0X5 1GB,UK.

When n was varied, maximum SHG was observed for n=4, with the signal decreasing thereafter. The result implied substrate surface effects promoted noncentrosymmetric morphology in the films, with the effect decreasing with larger numbers of bilayers. When the films were heated, the SHG signal decreased to the signal seen for n=1, showing chromophore orientation was retained in the first layer.

A detailed investigation of the mechanism of SA has been performed by Stuart and his research group[22]. They measured the ζ-potential of monodisperse colloidal silica particles in the presence of charged polymers. Colloidal silica particles had a net negative charge and ζ-potential. They formed the multilayer $(PVI/PAA)_2$ onto the silica particle, with measurement of the ζ-potential and hydrodynamic radius at each step(Fig. 15).

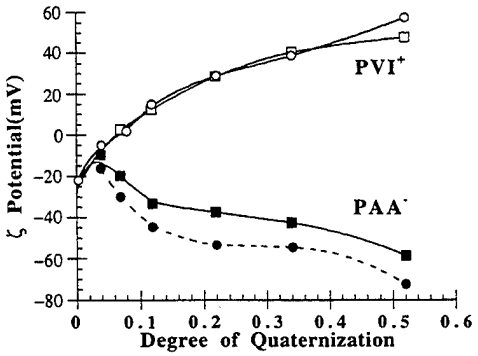

Figure 15. ζ-potentials of silica particles after addition of PVI^+(open squares), PAA(filled squares), PVI^+(open circles) and PAA(filled circles). Abscissa is the degree of quaternization of cationic PVI^+, a measurement of the proportion of charged groups. Adapted with permission from reference [**22**]. Copyright 1996 American Chemical Society.

With addition of highly charged PVI, the ζ-potential became highly positive. With addition of PAA the ζ-potential became highly negative.

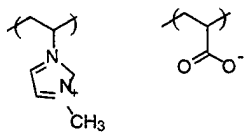

PVI PAA

XXII-XXIII

The changes were the same with subsequent bilayer formation. The results demonstrated that addition of the oppositely-charged polyelectrolyte caused strong overcompensation of the surface charge. The overcompensation of charge is a fundamental reason why polyion multilayer films can be prepared. Multilayer formation onto a silica or titania substrate was monitored by reflectance measurements. By systematically varying the charge on PVI, the effect of charge on adsorption was determined. The ζ-potential of colloidal silica was a function of counterion charge. No adsorption onto a PAA monolayer was observed when the PVI's average charge/monomer, $d_q = 0$. Significant adsorption occurred when $d_q = 0.5$. Similar behavior was observed in the PAMA/PMA system when charge was varied with increasing pH, causing deprotonation of the cationic PAMA.

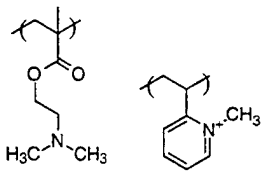

PAMA PVP

XXIV-XXV

From reflectance measurements, the stoichiometry of multilayer formation was determined(Table III).

Table III

Ionic Strength Effects on $(PSS/PVP)_n$ and $(PSS/PAMA)_n$ films[a]

System	I[b]	Γ_+[c]	Γ_-[d]	Stiochiometry[e]
$(PSS/PVP)_n$	0.005	0.56	0.35	2.7
$(PSS/PVP)_n$	0.1	2.18	1.13	3.2
$(PSS/PAMA)_n$	0.005	0.26	0.34	1.0
$(PSS/PAMA)_n$	0.1	0.80	0.94	1.1

[a]Reprinted in part with permission from reference [22]. Copyright 1996 American Chemical Society.
[b]Ionic strength of KNO_3 in all solutions.
[c]Adsorbed amount per layer of polycation(mg/m^2).
[d]Adsorbed anount per layer of polyanion(mg/m^2).
[e]Ratio between the number of cationic and anionic charges on the polymers in the multilayer.

In the PVP/PSS system the ratio between cationic and anionic charges was ~3. This value was independent of ionic strength and pH, although the amount of both polymers adsorbed increased with ionic strength. In contrast, the PAMA/PSS system had a stoichiometry of ~1. From these results, it appears that the type of polymer influences the stoichiometry. For PAMA and PSS, the charge resides farther from the backbone than PVP, suggesting steric factors may influence stoichiometry. For electroneutrality, the rest of the charge must be compensated by small ions.

Hammond describes polymer microstructure formation by deposition of PDDA/PSS multilayers onto a monolayer template[12]. She used the technique of microcontact printing to prepare a template. The technique involves a poly(dimethylsiloxane) stamp molded from a photolithographic master to transfer 2.5 μm lines of hexadecanethiol or 16-

mercaptohexadecanoic acid onto a surface separated by 3.5 μm spaces. In order to prevent adsorption of the ionic polymers onto regions of bare gold, the gold substrates were then dipped into a 5 mM solution of an oligo(ethylene glycol)-terminated alkanethiol to cover the remaining gold regions. As the gold substrate was patterned with a COO^- regions, selective adsorption of polycations occured in these areas. Polymer ridging reflecting the patterning was observed in films containing high molecular weight polymers.

D. Systems Containing Dyes and Amphiphiles

1. Amphiphiles

Decher and Hong have prepared multilayers containing boladikation and boladianion[125, 126].

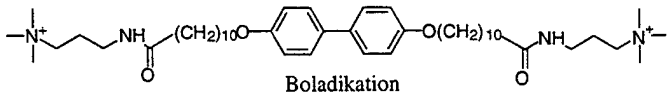

Boladikation

XXVI

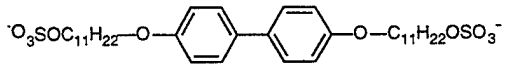

Boladianion

XXVII

Both of these molecules contain rigid biphenyl cores and long alkyl side chains with charged groups on the end. From UV/Vis measurements, linear buildup of material is shown. They demonstrate assembly of a 39 bilayer film composed of a monolayer of polymer PSS and 38 alternating layers of polycation PVDA and boladianion.

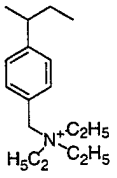

PVDA

XXVIII

Boladianion has a length 44.6Å in its extended conformation. Assuming it orients perpendicular

to the surface, 19 monolayers layers of boladianion have thickness 847Å. The calculated polymer layer thickness, 33Å, is in the range observed for other polymer systems. The bolaform amphiphile DIPY08 and the anionic polyelectrolyte PAMPSA have been investigated by AFM[19].

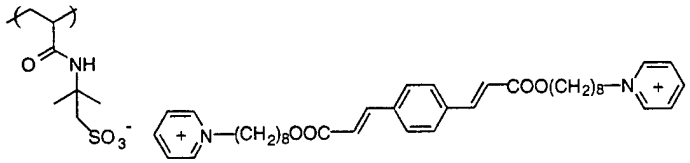

PAMPSA DIPY08

XXIX-XXX

The amphiphile was photopolymerizable by UV radiation. It took less than 5 min to dissolve a film in chloroform. Following photopolymerization immersion of the film in chloroform for 2 h caused only partial film removal. The diacetylene-containing amphiphile DCDS has been photopolymerized after being placed into an PMF film[25, 72].

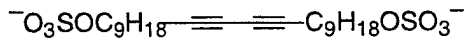

DCDS

XXXI

Following UV irradiation, the film turned red and a broad absorption appeared in the visible at 536 nm, indicating formation of a conjugated polymer backbone. Azobenzene-containing polymeric thin films containing the bolamphiphile PyC_6BPC_6Py showed pH effects on film morphology[16, 127].

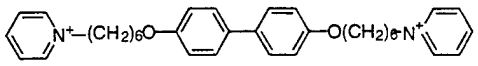

PyC_6BPC_6Py

XXXII

The polymer contained both sulfonic acid and carboxylic acid groups. When the pH was 4, the carboxylate groups were protonated and only the sulfonate groups contributed to the binding. When the pH of the bolamphiphile solution was 10, both the carboxylate groups and the sulfonate groups on the polymer surface had a negative charge, so the positively charged bolamphiphile bound to both groups. X ray diffraction measurements gave evidence for pH-dependent morphology changes.

The bolamphiphile PyC_6BPC_6Py has been used to prepare multilyers consisting of negatively-charged porphyrins(TPPS) and phthalocyanines(Cu-PTSA)[128]. In order to prepare a chemically-modified electrode, a multilayer consisting of Co-PTSA and the bolamphiphile PyC_6BPC_6Py adsorbed on a 3-mercaptopropionic acid modified electrode was prepared[129]. CV data demonstrated that the phthalocyanine deposited on the electrode could catalyze the oxidation of glucose. For 1-5 bilayers and a fixed glucose concentration, the anodic peak current was proportional to the number of bilayers the signal with leveling off at 6 bilayers. The proportionality reflected increased availability of sites for catalytic oxidation of gluose. Thicker films inhibited the diffusion of glucose into sites near the electrode. The anodic peak current was directly proportional to glucose concentration in the range 1-5 mM and to the square root of scan rate, showing the electrode process involved glucose diffusion. Under flow injection conditions, the detection limit for glucose was 150 pmol. A closely-related system for the detection of copper(II) ions involved multilayers containing Cu-PTSA and the bolamphophile PyC_6BPC_6Py has been described[130].

2 Dye Systems

Multilayers containing up to 30 porphyrin bilayers CuTPPS/ZnTPyBBCR have been prepared[86].

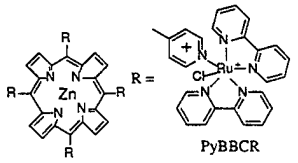

XXXIII

CV measurements on electrodes modified with these films gave a reversible 0.94 Vwave and had the ability to photocatalytically reduce O_2. The photoaction spectra of the films showed a photocurrent profile mirroring the film absorption spectrum. Under backside illumination, the phtocurrent intensities increased with thickness. Action spectra obtained under frontside illumination did not show the proportionality, showing the photoactivity was confined to layers next to the ITO/film interface.

Films composed of dyes/polypeptide multilayers have been prepared[38]. The plate-shaped dye Cu-PTSA

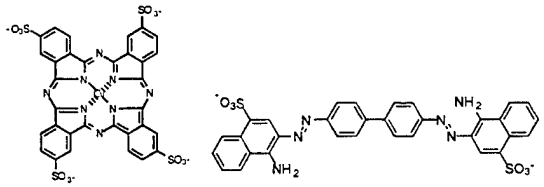

XXXIV-XXXV

and the rod-shaped dye CR form multilayers with the polypeptide PLL. Films composed of up to 100 bilayers of Cu-PTSA and PLL have dye aggregation changing with increasing number of bilayers. The UV/Vis spectra can be used to probe chromophore complexation. Figure 16 shows UV/Vis spectra of $(Cu\text{-}PTSA/PLL)_n$ films.

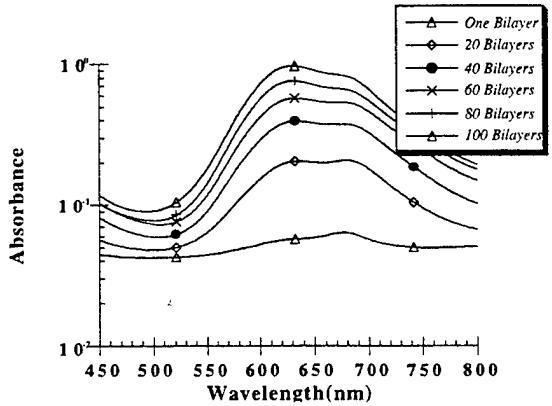

Figure 16. Absorption spectra of $(CuPTSA/PLL)_n$ films adsorbed onto a silanized glass substrate. Reprinted with permission from reference [38]. Copyright 1995 American Chemical Society.

The shape of the Q band of the absorption spectrum changed with increasing number of bilayers. The spectral changes resulted from variations in Cu-PTSA monomer and dimer proportions with increasing number of bilayers. Figure 17 shows plots of mole fraction monomer as a function of the number of bilayers for phthalocyanine-containing films.

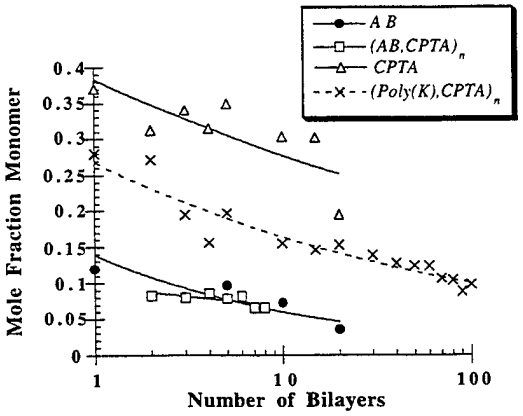

Figure 17. Mole fraction monomer as a function of the number of bilayers for a series of phthalocyanine-containing films. AB: Alcian Blue, CPTA: Cu-phthalocyanine tetrasulfonate, poly(K): poly(L-lysine). Reprinted with permission from reference [38]. Copyright 1995 American Chemical Society.

In all systems the monomer content decreased with increasing number of adsorption cycles. The monomer mole fraction varied with the nature of the oppositely-charged species. The highest fraction of monomer appeared in Cu-PTSA monolayers, with decreasing proportion when bound to PLL and the lowest proportion when bound to the positively-charged phthalocyanine alcian blue. The phthalocyanine layers have increased monomer content near the substrate, reflecting deposition of less material with only a few deposition cycels. Similar observations were made with multilayers composed of oppositely-charged porphyrins[86]. Films of up to 20 bilayers of CR and PLL also show changes in the dye absorption spectrum near the substrate, with the λ_{max} shifting from 498 to 506 nm as the number of bilayers increases from 1 to 20. Red shifts can be interpreted as J aggregate formation. Both types of films show intense dye optical activity, with films containing Cu-PTSA showing negative induced circular dichroism and CR showing positive circular dichroism.

Table IV has data describing PLL conformation changes occurring during adsorption and illustrates self-assembly(Section IIA) processes occurring during the PMF formation. The polypeptide had a coil conformation when in aqueous solution. The 1, 654 cm^{-1} amide I band obtained from FTIR spectra of dried film material shows a coil-to-helix transition occurring at some point during a polypeptide adsorption cycle.

Table IV

Polypeptide conformation changes following adsorption onto a surface and film drying[a]

System	CD Band I[b]	Amide I band[c]
PLL	202(-19,200)[d]	1,655
PLL,CR	197(-10,600)[e]	1,654
PLL,Cu-PTSA	202(-1,700)[f]	1,653

[a]Reprinted with permission from reference [38]. Copyright 1995 American Chemical Society.

[b]CD spectra of complex in neutral deionised water.

[c]Amide I frequency(cm^{-1}) obtained from FT IR spectra of thin film sample in KBr pellet.

[d]Wavelength of maximum CD in nm. Quantity in parenthesis is molar ellipticity in deg-cm^2-$dmol^{-1}$.

[e]Solution CD spectra were obtained from monomer molar ratio 0.6:1.0 poly(K),CR complex.

[f]Solution CD spectra were obtained from monomer molar ratio 0.25:1.0 poly(K),CPTA complex.

The dye CR has a pH-sensitive UV/Vis spectrum. This property has been applied by preparing PAH/CR multilayer coated glass as a pH-sensitive coating[90]. Anionic or cationic porphyrin/polymer films with PAH or PMA are also described.

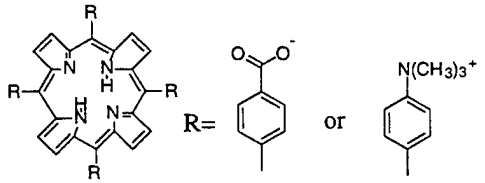

XXXVI-XXXVII

Thin films containing dyes with absorption bands in the near IR were also described. In particular, linear growth of a multilayer $(IR125/PAH)_n$ was demonstrated.

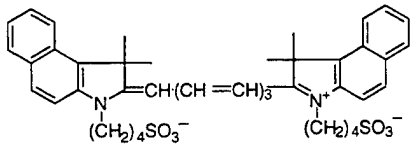

IR 125

XXXVIII

An extensive series of dye and polymer multilayers have been characterized by the QCM technique[73]. The *in-situ* QCM measurement shows dye adsorption occurs at a rate similar to

polymer adsorption. By estimating film thickness from the QCM frequency shift and comparing the result with the dye molecular dimenstion it was demonstrated that molecular size and charge affected the bilayer dimension. Certain dyes(CR and IC) oriented with their long axis perpendicular to the substrate while others(PS, AR26 and AR27) exhibited side-on orientation.

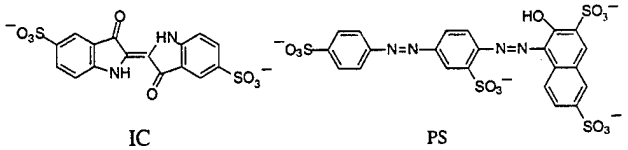

IC PS

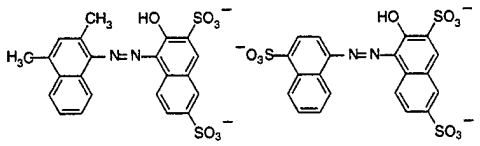

AR26 AR27

XXXIX-XLII

The porphyrins stood on the polymer surface in a packed card formation. One porphyrin(TPPS) had a bilayer thickness significantly larger than the film dimension.

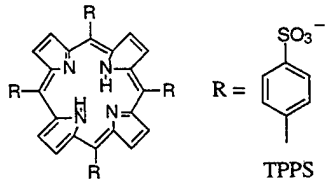

TPPS

XLIII

The UV/Vis data suggested the porphyrin ring became protonated when the film was immersed in solution, leading to dimer formation and a resulting thicker layer. Ariga suggests a mechanism for dye adsorption[73]. When the dye adsorbs onto the film surface, at least one charged site interacts with the outer solution phase, while the other charged sites bind to the polymer surface. The dye orientation with respect to the film plane results from minimizing hydrophobic interactions with the solution and ensuring electrical neutrality.

An example of a system showing a systematic relationship between structure and thin film properties is described by Tieke and his research group[131]. They synthesized two DPP derivatives and prepared thin films with PAH and other polymers as polycations(Fig. 18).

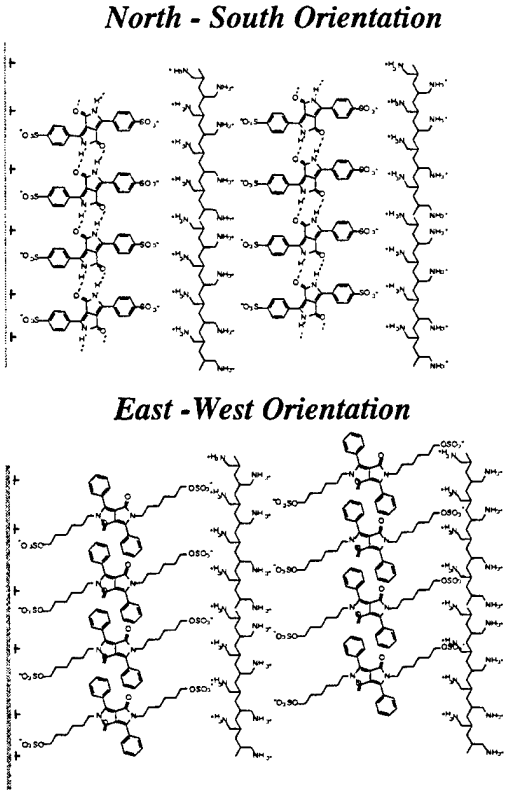

Figure 18. Schematic of north-south and east-west DPP-containing films.

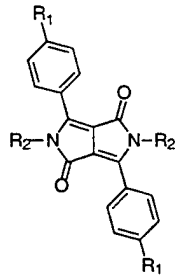

DPP

XLIV

The two compounds differed by the position of the sulfate and sulfonate groups. The anionic groups were either attached to the phenyl rings of the chromophore(north-south substitution: R_1 = SO_3H, R_2 = H) or to the N-atoms of the chromophore through alkylene spacer groups(east-west substitution: R_1 = H, R_2 = $-(CH_2)_6OSO_3H$). Multilayers were built up from a silanized glass substrate and absorption spectra of the films taken. In both the north-south and east-west chromophore films, linear increase in absorbance with the number of bilayers was shown, but the absorbance increase per bilayer was nearly double in the east-west system. The absorption spectrum of multilayers containing the north-south chromphore showed splitting into two

absorption bands at 534 and 488 nm, while the films containing the east-west chromophore had a single absorption band with a maximum at 478 nm. The splitting observed in the north-south chromophore was attributed to formation of chains of intermolecular hydrogen bonding between the lactam NH of one molecule and the O atom of the neighboring molecule. The differing optical density per bilayer appeared to result from orientational effects, where the transition dipole moment of the north-south chromophore containing films were oriented perpendicular to the multilayer plane, while those of the east-wast chromophore containing films were oriented parallel to the multilayer plane.

E. Biopolymer and Protein-Containing Systems

1. Biopolymers

Polysaccharide-containing PMFs have been prepared[14]. Regular buildup of films containing cationic chitosan with PSS and anionic chondroitin sulfate with PDDA was demonstrated.

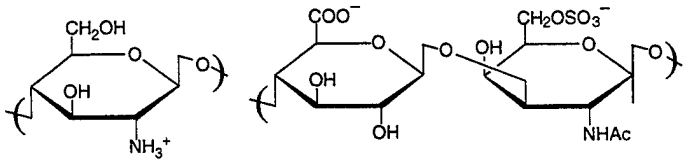

Chitosan Chondroitin Sulfate

XLV-XLVI

In (chitosan/PSS)$_n$, film thickness increased with dipping solution ionic strength, ranging from 15Å/bilayer when no salt was present to 69Å in 1 M NaCl. Adsorption kinetics were shown to be a function of ionic strength. Adsorption of chitosan did not saturate after 20 min in 0 M NaCl, but became saturated within 6 min with 0.25 M NaCl. Shielding of chitosan charge by the added salt gave more conformational flexibility, facilitating adsorption onto the surface. An example of a polymer/biopolymer hybrid prepared by this method is a film containing alternate layers of DNA and PAH[132, 133]. Films composed of the oppositely charged polypeptides PLL and PGA have been made[134]. From circular dichroism measurements, the polypeptides had a coil conformation in solution. IR analysis of the film material showed the presence of a β-sheet conformation resulting from self-assembly(Section IIA) between the two polypeptides during monolayer deposition.

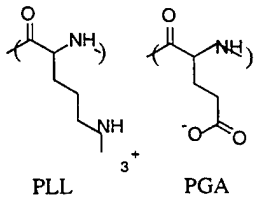

XLVII-XLVIII

2. Protein-containing Films

Hong[39] describes streptavidin-containing films. Prior to protein deposition, a precursor film $(PSS/PAH)_7$+ biotinylated-PLL was prepared. In order to prepare a film with in-plane structure, the film was irradiated with UV light through a copper mask. Following irradiation, the film was immersed into a solution containing FITC-labeled streptavidin. The UV radiation destroyed the unprotected film surface so that FITC-labeled streptavidin applied to the multilayer gave enhanced binding to areas protected from the UV light. The protein arrays were characterized with fluorescence microscopy. Areas protected from UV light showed strong fluorescence of adsorbed FITC-labeled streptavidin.

A group of detailed investigations[81, 135, 136] give information on the properties of protein-containing PMFs. Films were prepared from proteins with a wide molecular weight range, from Cyt c(MW 12,400) to catalase(MW 240,000) alternate with a wide variety of polymers and nanoparticles, including PAA, PAH, Mont, PEI, PDDA, PSS and the PAn derivative PAPSA.

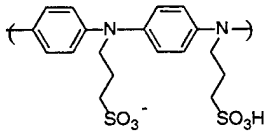

XLIX

Lvov demonstrates film formation from proteins with a wide isoelectric point range. Because lysozyme has an isoelectric point of 11, films deposited from a solution of pH 4 required the use of the negatively charged polymer PSS for the oppositely-charged component. No adsorption occured in dipping cycles using positively charged lysozyme and PAH. Cyt formed films with PSS, but not with PAH. In contrast, GOx, having an isoelectric point of 4.2, required the use of the positively-charged polymer PEI at the deposition pH equaling 6.5. An interesting example of the versatility of the technique is shown in Hb-containing films(Table V). Films were deposited

at a pH both above and below its isoelectric point(6.8). Films deposited below pH 6.8 used PSS as the counterion, while films depositied above pH 6.8 used PEI. Oppositely charged polymers are required for successful film preparation. The electrochemistry of the acidic Cyt b5/PLL bilayer has been investigated[137]. An $HS(CH_2)_7COOH$ layer was placed on gold, followed by a PLL layer and a Cyt layer. CV measurements gave a well-behaved and reproducible response attributed to electron transfer between the Au electrode and the adsorbed Cyt b5 through the alkane thiol and PLL layers.

Table V

Examples of Data Obtained for Protein-Containing Films[a]

Protein	pI[b]	pH used	Polyion	τ[c]	-Δf(Hz)	Thickness of Protein + Polyion Layer(Å)
Hemoglobin	6.8	4.5	PSS	4	1100+190	175+31
Hemoglobin	6.8	9.2	PEI	4	1200+60	82(bilayer)

[a]Reprinted in part with permission from reference [81]. Copyright 1995 American Chemical Society.
[b]Isoelectric point.
[c]Adsorption lifetime(min).

Kong[27] prepared a multilayer consisting of glucose isomerase and the bolamphiphile PyC_6BPC_6PY in porous trimethylamine polystyrene beads. Because the carrier pore diameter was 46 nm, only two layers of enzyme could be deposited into the pores. Enzyme activity was comparable to soluble and monolayer enzyme preparations. Glucose isomerase-containing multilayers also had enzyme activity[87]. Kong and his coworkers measured enzyme activity in films containing up to 40 enzyme layers. In the 40 bilayer film the average activity per layer decreased 50% of that measured for a 10 layer film. This effect was attributed to limitation in the ability of substrate to diffuse deeply into the film.

Albumin/heparin multilayers containing up to 5 bilayers have been prepared in order to develop actively nonthrombogenic surfaces[34]. Heparin binding to albumin preadsorbed on germanium has been measured as a function of time, pH and ionic strength. Kinetics of deposition were similar to other protein systems, reaching saturation after 20 min. Heparin is a polysaccharide containing negatively-charged sulfate groups. Albumin has an isoelectric point at about pH 4.9. The binding of heparin to an albumin-treated surface was a strong function of pH, with maximal binding at acidic pH. The pH profile mirrored the albumin acid titration curve. Heparin binding was a function of ionic strength. Maximum binding occured at moderate ionic strength, while in the absence of salt or in high salt concentration binding decreased. The

complex behavior reflected the ionic strength dependence of heparin conformation, with the polysaccharide being a stiff rod at low ionic strength and an extended coil at higher ionic strength. At very high ionic strength charges became screened, inhibiting electrostatic interactions. The amount of material deposited in multilayers increased in direct proportion to the number of deposition steps, with a constant ratio of albumin to heparin.

3. Complex Protein-Containing Films

Complex, multiple component protein-containing films have also been prepared by the SA technique. A Carnation Mottle virus-containing film was prepared having the deposition sequence $(PSS/PAH)_n$ + virus + $(PSS/PAH)_m$, with n=1-6 and m=1-6[89]. Analysis of the SAXR data gave insight into the film structure. The virus bound to and partially penetrated the polymer surface. The next layer filled holes between the virus and a smooth film surface returned. As an example of a film containing oppositely-charged proteins, Lvov[81] describes an attempt to prepare a LYS/GOx binary film. First he prepares a precursor film PEI/PSS/PEI+$(PSS/LYS)_2$. Even though GOx had a negative charge, it did not bind to LYS. By placing a bilayer PSS/PEI after the LYS layer, a $(GOx/PEI)_6$ multilayer successfully adsorbed to the film. This example illustrates differences between proteins and simple polyions. Proteins have specific tertiary structure with charged, neutral, polar and hydrophobic groups in specific locations on the surface rather than dispersed throughout a polymer. Because of the specificity of interaction between two proteins in a complex(for example, tropomyosin dimerization discussed in Section IIB), direct adsorption of a protein in solution onto a protein layer is not entropically favored. Use of a polyelectrolyte as a "polyion glue" (Lvov, Y. personal communication) gives nonspecific adsorption between polymer and protein layers. The authors give an example of a film containg two different positively charged proteins: $(PEI/PSS)_2$ + $(Mb/PSS)_2$ + $(Mb/PSS/LYS/PSS)_4$ and two negatively charged proteins: $(PEI/PSS)_2$ + $(PDDA/GOx)_2$ + $(PDDA/GOx/PDDA/GA)_5$. Finally, they demonstrated a protein/polycation/ceramic film: $(PEI/PSS)_2$ + $(PEI/Mont)_3$ + PEI + (GOX/PEI/Mont/PEI).

A chemically active two enzyme system formed from GOx and peroxidase(POD) has been prepared[138]. The film composition was $(PEI/PSS)_4$ + $(POD/PSS)_2$ + $(PEI/GOx)_2$. Enzyme activity in these films was monotored by adding glucose to the solution. GOx oxidized D-glucose to D-glucono-δ-lactone yielding hydrogen peroxide which is then used by POD to oxidize a dye to a colored form. A similar system was prepared on an ultrafilter[139]. A multilayer containing glucoamylase(GA) and GOx was assembled with PEI as the polycation PEI/PSS bilayers between the enzyme/PEI layers(Fig. 19).

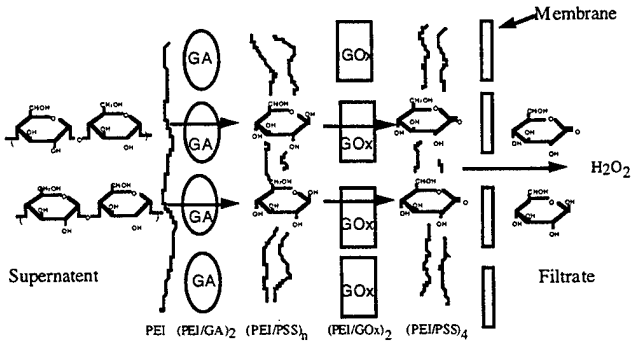

Figure 19. Schematic of GA and GOx-containing multilayer catalyzing breakdown of starch into D-glucono-δ-lactone[139]. Figure is not drawn to scale

The enzymatic activities of the films were evaluated by using pressure to force a starch solution through the ultrafilter and glucose and H_2O_2 assayed in the filtrate. They made five types of films(Table VI).

Table VI
Enzyme Multilayer Films Investigated for
Conversion of Starch to D-Glucono-δ Lactone[139]

Film	Composition
1	Filter + $(PEI/PSS)_4$ + $(PEI/GOx)_2$ + $(PEI/PSS)_2$ + $(PEI/GA)_2$ + PEI
2	Filter + $(PEI/PSS)_4$ + $(PEI/GOx)_2$ + $(PEI/PSS)_{10}$ + $(PEI/GA)_2$ + PEI
3	Filter + $(PEI/PSS)_4$ + $(PEI/GA)_2$ + $(PEI/PSS)_2$ + $(PEI/GOx)_2$ + PEI
4	Filter + $(PEI/PSS)_4$ + $(PEI/GA)_2$ + $(PEI/PSS)_{10}$ + $(PEI/GOx)_2$ + PEI
5[a]	Filter + $(PEI/PSS)_4$ + $(PEI/MIX)_2$ + PEI

[a]MIX is an equimolar mixture of GOx and GA in the dipping solution.

The highest starch conversion was observed in film 1, followed by film 2. In both of these films, the order of protein layers against the flow agrees with the order of enzymatic reactions. In films

3 and 4, the order of the two enzymes was reversed and lower yields were observed. Film 5 had the lowest yield, possibly due to lower GA adsorption. A spacer layer effect was also observed. Film 2, having a 10 bilayer spacer layer, exhibited greater activity than film 1, having a 2 bilayer spacer. The authors speculate the shorter spacer layer promoted product inhibition of GA by gluconolactone.

An enzyme multilayer containing GOx and GA was prepared on a gold electrode[37]. After derivatizing a gold surface with 3-mercaptopropionic acid, a layer of NC_6BPC_6N was added to give the surface a positive charge.

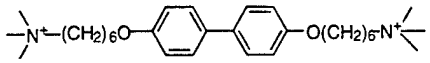

NC_6BPC_6N

L

The bienzyme film consisted of repeating bienzyme units $(GOx/NC_6BPC_6N + GA/NC_6BPC_6N)_n$. The sensor succesfully detected maltose over a range 1-10 mM. Binding of the enzymes to the gold surface was necessary. A control experiment with the free enzymes, substrate and electrode in solution could not detect maltose. An electrocatalytically active enzyme/mediator structure has been assembled[26]. Multilayers containing GOx and ferrocene-modified PAH(designated as PAH-Fc) were assembled on mercaptopropanesulfonate modified gold electrodes and characterized. GOx catalysis was mediated by the ferrocene derivatized polymer where electrically-mediated ferrocene oxidation and reduction couples with GOx according to

$$PAH\text{-}Fc \rightarrow FAH\text{-}Fc^+ + e^- \quad (17)$$

$$2PAH\text{-}Fc^+ + GOx(FADH_2) \rightarrow GOx(FAD) + 2PAH\text{-}Fc \quad (18)$$

$$GOx(FAD) + \text{glucose} \rightarrow GOx(FADH_2) + \text{D-glucono-}\delta\text{-lactone} \quad (19)$$

When a potential was applied, PAH-Fc oxidized to $FAH\text{-}Fc^+$ and a catalytic current paralleling the oxidation of glucose was observed. The steady state glucose catalytic oxidation current was directly proportional to the number of bilayers. To determine the proportion of GOx molecules efficiently coupled to PAH-Fc, the catalytic current was measured in the presence of ferrocenesulfonate. The 3- to 10- fold increase in catalytic current suggested a large proportion of GOx was enzymatically active but poorly coupled to the mediator.

Antibody-containing PMF films have been developed[20]. The interaction of IgG and anti-IgG on a precursor $(PAH/PSS)_2$ multilayer was investigated by QCM(Table VII). When either IgG or anti-IgG was placed onto the multilayer, the QCM mass change was ~60 ng, suggesting the multilayer had the same affinity for either species. When IgG was added to a $(PAH/PSS)_2$ + anti-IgG multilayer, ~35 ng adsorbed. In contrast, when anti-IgG was added to a $(PAH/PSS)_2$ + IgG multilayer, ~91 ng adsorbed. The orientation of anti-IgG on the film surface controlled the binding. The anti-IgG F(ab) receptor sites had to be accessible to IgG in order for binding to occur. In contrast, the binding of anti-IgG from solution onto bound IgG had less orientation effect as the F(ab) receptor sites could bind to IgG. The results illustrate the specificity of protein-protein interactions(Section IIA, B) *vs.* nonspecific electrostatic interactions(Section IIC). When BSA was incubated with an IgG or anti-IgG treated film, subsequent binding of the anti-IgG or IgG was inhibited 10%, showing there was minimal nonspecific binding in these films.

Table VII

Mass changes for IgG or anti-IgG bound onto a $(PAH/PSS)_2$ coated QCM electrode

First Layer	Δm(ng)[b]	Second Layer	Δm(ng)
anti-IgG	64±3	IgG	35±3
IgG	58±3	anti-IgG	91±3

[a]Reprinted in part with permission from reference [20] Copyright 1997 American Chemical Society.
[b]Mass changes measured from QCM experiments.

F. Inorganic/Organic Systems

1. Colloidal Dispersions

The first published demonstration of the SA technique was described by Iler[69, 70]. His films were composed of colloidal boehmite alumina(AlO_2H) fibers with diameter 5-6 nm and colloidal silica with particle diameter ranging from 3-100 nm. The films had controlled, uniform thickness and interference colors. The observed colors were influenced by film composition and number of layers. For example, a film with two layers of 880Å polystyrene latex particles, each associated witha 100Å film of colloidal boehmite gave a light blue film. One layer of 2,640Å latex plus 100Å alumina gave a light yellow film. The wavelength of

maximum reflection could be varied from the number of layers of silica and alumina[70]. A two layer film had a reflectance maximum at 450 nm. With three layers it increased to 560 nm. A four layer film had a reflectance maximum of 625 nm. The interference colors observed in this system have analogy to the interference colors seen in mollusc shells(Section IIIB), as both systems are composed of multilayers placed down by an SA precess. Recently, the silical/alumina system has been investigated by the quartz microbalance[94]. They measured adsorption of 5-50 nm silica particles on a gold surface. QCM measurements demonstrated a constant uptake of material per deposition cycle. They found a 30s dip time to be sufficient for equilibration to occur. Mass uptake was significantly influenced by ionic strength but not by particle size. The ionic strength effect resulted from electrostatic screening of the charges on the particles, enhancing adhesion. The authors proposed that the film surface area and pore size could be varied by successive depositions of small and large particles from solutions with varying ionic strength.

Another study investigated multilayers of SiO_2 and polycations[95, 140]. QCM measurements on $(SiO_2/PDDA)_n$ films showed constant uptake of material per deposition cycle. The thickness of SiO_2/PDDA multilayers showed strong dependence on ionic strength and particle concentration. At a given SiO_2 particle diameter, the amount of material deposited increased with SiO_2 weight concentration. When the weight concentration was 0.1 mg/ml, there was no effect of particle diameter on the amount of material deposited. At higher concentrations, the amount of material deposited increased with SiO_2 particle diameter. For example, at a SiO_2 concentration of 100 mg/ml, a QCM frequency change of -700 Hz/deposition step was measured, but when the diameter was 78 nm, the frequency change was -2,500 Hz/deposition step. The amount of SiO_2 deposited per adsorption step was constant for a dip time ranging from 0.25 min to 20 min. The amount of material deposited increased with ionic strength. At low ionic strength, less than one SiO_2 monolayer was deposited per adsorption step. At an ionic strength of 0.3M, approximately 2 SiO_2 monolayers were laid down per deposition step. At higher ionic strength charges on SiO_2 were neutralized, facilitating deposition of mote material. In all experiments, the measured mass of SiO_2 *vs.* the mass of PDDA deposited per layer showed excess PDDA, with the relative amount of PDDA adsorbed increasing with ionic strength. The authors attributed this behavior to the ionic strength dependence of PDDA conformation where PDDA behaved as a linear polyion extended chain at low ionic strength and a coil at high ionic strength. The electrostatic interaction of SiO_2 and PDDA was investigated by turbidity measurements of IPEC complexes in solution. Turbidity was maximum at [SiO2]/[PDDA] = 64 (w/w). Comparison of QCM and turbidity measurements indicated that PDDA's positive charge was not completely neutralized by SiO_2 negative charge during monolayer adsorption. The

result suggests the PDDA/SiO_2 complex contained polymer loops not adhering to the SiO_2 surface. PDDA/SiO_2 IPEC complexes were prepared in solution and adsorbed onto the multilayer. By varying the SiO_2/PDDA ratio, the complex could be either be positively or negatively charged and adhered to an appropriately-charged surface. Complex films showing reproducible deposition per layer were prepared, including (SiO_2(45 nm diameter)/PDDA + SiO_2(25 nm diameter)/PDDA)$_n$ and (SiO_2/PDDA + GOx/PDDA)$_n$.

2. TiO_2 films.

A cationic TiO_2 complex was prepared by the addition of $TiCl_4$ to 6 N HCl, yielding a stable colloidal dispersion[113]. (TiO_2/PSS)$_n$ multilayers were prepared up to n=60. The films showed linear increase in UV absorbance with n but retained high visible transparency. Advancing contact angle measurements showed regular oscillation between 37 and 22 deg as the topmost layer was PSS or TiO_2. Electrostatic deposition was clearly demonstrated by XPS. When a TiO_2 layer was placed on a PSS surface, the XPS spectrum showed a clear Ti peak. In contrast, when TiO_2 was adsorbed onto a positively charged silanized surface, no Ti peak appeared. Kotov describes photocurrent measurements in a series of polyelectrolyte/semiconductor nanoparticle multilayers[84]. A multilayer (PDDA/TiO_2)$_n$ behaved like an n-type semiconductor, where upon illumination, had a photocurrent caused by photogenerated holes and water oxidation at the electrode surface. The magnitude of photocurrent could be controlled by insertion of insulating layers. The film (TiO_2/PDDA)$_n$ had a photocurrent directly proportional to n. A Mont layer inserted into the multilayer behaved like an insulator, causing the photocurrent to decrease. A correlation between the position of Mont layers and photocurrent appeared. A series of films (TiO_2/PDDA)$_n$ + (Mont/PDDA)$_3$ + (TiO_2/PDDA)$_m$, where n=0-10 and m+n=10, were prepared. The Mont layers divided the film into active and inactive parts. The photocurrent was also directly proportional to n, with the layers above the insulator layers being inert.

3. Colloidal Gold

Fan describes a system containing gold nanoparticles, dendrimers and sol-gel glass[35]. Colloidal gold was prepared from the reduction of $HAuCl_4$ by citrate ion in aqueous solution. A deposition cycle involved preparation of two G_4 PAMAM dendrimer/colloidal gold bilayers, followed by dip coating into a silca sol solution. After several deposition cycles, the samples were calcined to remove the dendrimers, giving porous composite films. TEM images show a regular array of 20 nm diameter gold particles spaced at 30 nm interval in the silica sol-gel matrix. A similar colloidal gold-containing system is described by Schmitt[141]. They prepared

a series of films having the composition PEI + $[(PSS/PAH)_m + (Au/PAH)]_4$. X-ray reflectivity measurements from films with m 3 showed multiple Bragg reflections, giving evidence for periodic layers of gold nanoparticles whose spacing could be changed by varying m. Similarly, UV-vis spectroscopy showed variation in peak maxima as m increased from 0-3. The absorption maximum λ_{max} = 660, 600 and 550 nm for m = 0-2, with no additional changes with larger m. The increased spacing eliminated the induced dipole interactions that gave rise to the long wavelength absorption bands.

4. Semiconductor Particles

An anionic PbI_2 hydrosol was synthesized by addition of slightly twofold excess I^- to lead nitrate[142]. Multilayers were prepared with the cationic bolamphiphile PyC_6BPC_6Py : $(PbI_2/PyC_6BPC_6Py)_n$ Uv-vis spectra showed linear increase in material deposited with number of deposition cycles. X-ray diffraction measurements gave a d spacing of 6.7 nm. From TEM, the average PbI_2 particle size was determined to be 3.8 nm and assuming the thickness of the amphiphile monolayer to be 3 nm, the film contains altenating hydrosol and amphiphile monolayers. By solubilizing CdS with mercaptoacetic acid, multilayers with the polycation I-6-$MeBF_4$ have been prepared[143].

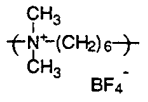

I-6-Me-BF_4

LI

The S-H group of mercaptoacetic acid reacted with the CdS particles, leaving the COO^- groups on the surface. Linear buildup of material per deposition cycle was confirmed by QCM and UV-vis spectroscopy. TEM and X-Ray diffraction measurements confirmed the alternating nanoparticle/polymer multilayer structure. Alternating layers of polyelectrolye-semiconductor nanoparticles have been described by Fendler[8], including $(PDDA/CdS)_n$ and $(PDDA/graphite\ oxide)_n$ films. $(PDDA/CdS)_n$ films exhibited fluorescence(λ_{max} 490 nm) with intensity proportional to n. X-ray diffraction measurements gave a d spacing of 6.5 nm, corresponding to 4 nm CdS particle layer and 2.5 nm polymer layer. Graphite oxide-containing films were prepared by using exfoliated graphite oxide sheets. Multilayer formation was demonstrated with surface plasmon spectroscopy. X-ray diffraction measurements showed one PDDA/graphite oxide bilayer to have 3.8 nm thickness. The graphite oxide containing films were converted to graphite by chemical or electrochemical reduction.

5. Clay Minerals

Multilayers composed of a PDDA and individual sheets of the mineral hecotorite[$Si_8(Mg_{5.5}Li_{0.4}H_{4.0}O_{24.0})^{-0.7}Na^{+0.7}_{0.7}$] have been prepared. When stirred in water, this silicate mineral exfoliated into negatively charged, two-dimensional sheets 25-35 nm in diameter and 1 nm thick. Similarly, montmorillonite(Mont = $Na_{0.66}(OH)_4Si_8(Al_{3.34}Mg_{0.66})O_{20}$)[15], when placed in water and sonicated forms a dispersion of negatively charged 1x500x500 nm sheets. Both $(PDDA/hectorite)_n$[78] and $(PDDA/Mont)_n$[15] films showed linear buildup of film thickness with number of deposition cycles. Lvov observed a concentration dependence in the kinetics of Mont deposition. At 0.03% Mont concentration, the adsorption time was 1.8 min. At 1% concentration, saturation of adsorption does not occur after 12 min. Observation of the physical state of mixtures of Mont and PEI suggested gel formation occured at the high Mont concentration. An investigation of the effect of defects on film growth was performed by investigation of $(PDDA/hectorite)_n$ films[143]. Following initial poor deposition, film growth occurred even on substrates treated with hydrophobic materials. To account for these observations, it was proposed that PDDA and hectorite adsorbed at isolated imperfections in model inert surfaces, forming islands that grow to coalescence. The results demonstrated that SA film growth can heal defects that appear during film growth.

6. Phosphate/Phosphonate Systems

Metal phosphonate salts have unique properties allowing their use in PMFs[144]. They form layered structures where the metal ions and phosphonate oxygen atoms arrange in puckered sheets. A structural motif of these sheets is a planar network of tetra- or divalent metal ions. The most commonly used salt is α-zirconium phosphate($Zr(HOPO_3)_2 \cdot H_2O$), abbreviated as "α-ZrP".

Keller[31] describes films containing α-ZrP salts. The α-ZrP sheets can be used in PMFs because the acidic protons of α-$Zr(HPO_4)_2$ can be exchanged with TBA^+. This was accomplished by titration with 0.5M TBA^+OH^- to pH 8.5. The titration caused complete exfoliation and single, separate layers could be suspended indefinitely in water. When in the presence of a positively charged surface, TBA^+ went into solution, and the sheet adsorbed to the surface. The loosely-bound TBA^+ ions on the surface facing the solution can then be displaced by other cations, forming the next layer. Clear, high optical quality films with constant layer thickness was demonstrated in $(\alpha\text{-ZrP/PAH})_n$, $(\alpha\text{-ZrP/Cyt c})_n$ and $(\alpha\text{-ZrP/Al}_{13}^{7+})_n$

films, where $Al_{13}^{7+} = Al_{13}O_4(OH)_{12}(H_2O)_{24}^{7+}$. Keller also describes repeating four layer structures having the composition (α-ZrP/PAH + $K_2Nb_6O_{17}^{2-}$ /PAH)$_n$ and (α-ZrP/Al_{13}^{7+} + α-ZrP/PAH)$_n$. As with the simpler films, regular film growth was observed in these more complex structures.

Photoinduced charge separation has been investigated in redox polymer-containing multilayers[145]. With the goal of developing systems that undergo mimic photosynthesis, the authors adsorbed various multilayers onto silanized fumed silica particles. Excitation of the bilayer film SiO_2/α-ZrP/PVRu(II) at 532 nm showed a photoinduced metal-to-ligand charge transfer state PVRu(II)* localized on the polymer.

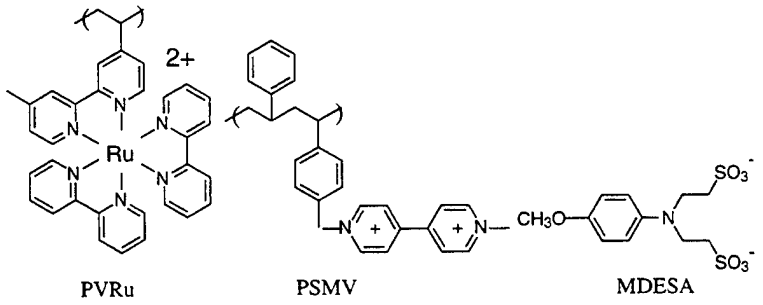

PVRu PSMV MDESA

LII-LIV

The film SiO_2/α-ZrP/PSMV(2+) + α-ZrP/PVRu(II) had similar behavior, indicating the intervening α-ZrP sheet inhibited photoinduced electron transfer to the viologen layer.

When the reversible electron donor $MDESA^{2-}$ was added to the soluton, observation of spectroscopic transients associated with the viologen radical cation and $MDESA^{\bullet -}$ gave evidence the reaction

$$MDESA^{2-} + PVRu(II)^* \rightarrow MDESA^{\bullet -} + PVRu(I) \quad (18)$$

occured, followed by the facile viologen reduction

$$PVRu(I) + PSMV^{2+} \rightarrow PVRu(II) + PSMV^{\bullet +} \quad (19)$$

The reactions yielded a charge-separated state of oxidized solution-phase MDESA and reduced MV^{2+}, stabilized in the inner layer of the composite. The reduced $PSMV^{\bullet +}$ species decayed with second order kinetics, consistent with rapid cage escape of $MDESA^{\bullet -}$ followed by diffusion

to a reduced PSMV site. In contrast the composite SiO_2/α-ZrP/PVRu(II) + α-ZrP/$PSMV^{2+}$ showed no photo-oxidation of MDESA or reduction of $PSMV^{2+}$, demonstrating the multilayer structure inhibited interaction between Ru(II)* and $MDESA^{2-}$. The film SiO_2/PSS/$PSMV^{2+}$ + PSS/PVRu(II) showed no photo-oxidation of $MDESA^{2-}$, suggesting a strong interaction between PSS and Ru(II) inhibited interaction with $MDESA^{2-}$. When PVRu(II), $PSMV^{2+}$ and $MDESA^{2-}$ were dissolved in solution, photo-oxidation of $MDESA^{2-}$ occurred, but no reduction of $PSMV^{2+}$ was observed, presumably from electrostatic repulsion between the two polycations. Finally, no photochemistry occured in the film SiO_2/α-ZrP/$PSMV^{2+}$ + α-ZrP/PAH, eliminating any interaction between PS MV^{2+} and $MDESA^{2-}$ causing the observed photochemistry.

The SA technique has been used to construct metal-insulator-gold nanocluster-insulator-metal(MINIM) structures[32]. Because the gold nanoparticle placed in the structure has a small diameter(25Å), the device allowed the observation of single electron charging effects at ambient temperatures. To assemble the MINIM device, the authors primed a gold substrate with 2-mercaptoethylamine. Insulating layers of α-ZrP and PAH were added until a multilayer terminated by cationic PAH of thickness 30-100Å was prepared. The substrate was then placed into an aqueous solution of 25Å citrate-stabilized gold particles for 12 hours. Another insulating PAH/αZrP multilayer was adsorbed in reverse order onto the gold layer. To complete the MINIM structure, a thin layer of $FeCl_3$ was deposited on the surface and the film was exposed to pyrrole vapor. Following polymerization to poly(pyrrole), the $FeCl_3$ layer was removed by washing with 95% ethanol. XPS data gave Au/Zr, Au/Si and Zr/Si intensity ratios consistent with a sandwich film structure where Au nanoparticles were embedded between two insulating layers. An i-V curve for an [$(\alpha\text{-ZrP/PAH})_2$/ + Au + $(\text{PAH/}\alpha\text{-ZrP})_2$ + poly(pyrrole)] device showed a high impedance region on both sides of 0 V, representing the average charging potential of each particle of the double junction array by a single electron. At higher voltage, facile tunneling of electrons through the device resulted in a square law dependence of the current rise on either side of the gap. A device without the gold layer showed a linear i-V curve typical of a resistor. By changing insulator layer thickness from 80 to 30Å the gap width changed from 400 to 275 mV. This work demonstrated how the SA technique could be used to control the spatial organization and electronic properties on the nanometer level.

7. Other Inorganic Systems

Another example of a redox system is described by Lowy and Finklea[76]. They prepared numerous gold electrodes having polyion multilayers and electrostatically bound redox couples. Strength of redox couple binding was measured by the rate of loss of CV peak area

over multiple scans. An example of a strong binding system was ferrocyanide bound to a self-assembled cationic monolayer of 4-(aminomethyl)pyridine-11-mercaptoundecanoamide. Less than 35% of the ferricyanide redox couple was lost from the electrode after 110 scans. A small peak separation gave evidence that the redox couple exhibited nearly reversible behavior. The authors used the electrostatic self-assembly technique to constrct a two-terminal sensor system bound to the same electrode surface. CV was used to monitor formation of the redox centers. First, a self-assembled monolayer of 11-mercaptoundecanoic acid was deposited on a gold flag(Fig. 20A).

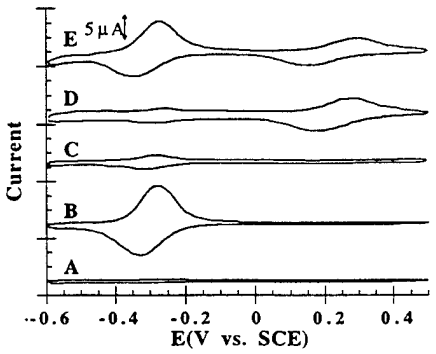

Figure 20. CV data obtained during five stages of assembly of a sensor with both the reference and sensor redox couples were attached to the same electrode. A: A self-assembled monolayer of 11-mercaptoundecanoic acid deposited on a gold flag. B: an iron(II) redox couple C: $PVPMe^+$ was attached to the Fe(II) redox couple. D: ferrocyanide was adsorbed to the outermost cationic layer. E: The system was soaked in ferroin solution. Figure adapted with permission from D. Lowy and H. Finklea *Electrochimica Acta* **42**, 1325, (1997), Copyright 1997 with permission from Elsevier Science, The Boulevard, Langford Lane, Kidlington 0X5 1GB, UK.

The CV showed no bands. Second, an Fe(II) redox couple was adsorbed onto the carboxylate groups from ferroin solution(Fig. 20B). Third, $PVPMe^+$ was attached to the Fe(II) redox couple, causing loss of most of the iron redox wave(Fig. 20C).

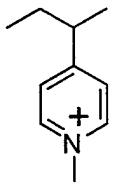

$PVPMe^+$

LV

Fourth, ferrocyanide was adsorbed to the outermost cationic layer, confirmed by the appearance of the ferrocyanide wave(Fig. 20D). Finally, the Fe(II) redox couple was regenerated by soaking

the system in ferroin solution(Fig. 20E). The CV showed two waves, corresponding to the two redox couples in the multilayer. This system was used for pH measurement. The formal potential of the new iron couple shifted in a Nernstian fashion with the proton concentration while the ferricyanide couple kept a stable potential over neutral and alkaline pHs. Thus, the multilayer behaved as a pH sensor with an internal reference.

Multilayers containing polyoxometallate have been prepared[24]. Initially, a polyanion was adsorbed onto a glassy carbon electrode, followed by adsorption of a polycation. Immobilised polyanions(isopolymolybdate, phosphotungstate and silicotungstate) had redox properties similar to their solution form. Cations that formed precipitates with the polyoxometallates in solution tended to solubilize the anions, leading to poor film formation. Polymeric cations like PVP^+ performed well. In particular, a protonated $(PVP/silicotungstate)_4$ film was proposed for use as a coherent insulating coating and was capable of efficient charge mediation within the multilayer.

G. Variations on the Sequential Adsorption Technique

1. Based on non-electrostatic forces

PAn multilayers utilizing hydrogen bonding interactions have been prepared[146]. PAni forms bilayers with water-soluble polymers PVA, PVP, PEO and PAAm.

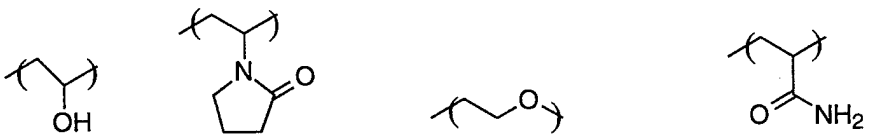

PVA PVP PEO PAAm

LVI-LIX

In comparison with PSS/PAn multilayers, films based on hydrogen bonding had a greater density of loops and tails. The films exhibit conductivities about 1 order of magnitude higher than PMF films. Although useful in PAn films, attempts to prepare other multilayers via hydrogen bonding yielded inconclusive results.

Multilayers held together by charge transfer interactions have been prepared[103]. The charge transfer donor polymer was PCzEMA and the acceptor polymer was PDNBMA

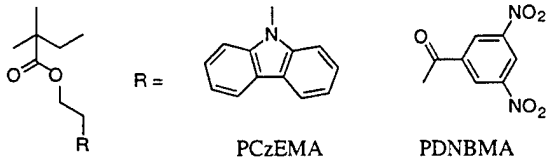

LX-LXI

Both polymers had no charge and were soluble in methylene chloride. The substrate dip time was 5 min, with a 10 min methylene chloride rinsing step in between dips. Multilayer buildup was demonstrated by surface plasmon resonance spectroscopy. An absorption spectrum of a six bilayer films showed broad absorption band up to 600 nm reflecting charge transfer complex formation between donor and acceptor monolayers.

By forming a complex between the primary amine functionality of the dendrimer G_6 PAMAM, and Pt^{2+}, dendrimer-containing multilayers have been assembled[147].

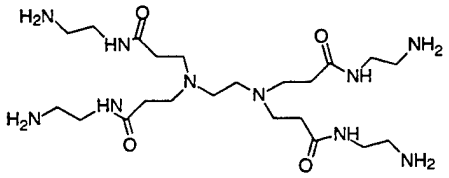

LXII

Angle-dependent XPS measurements confirmed the multilayer structure of these films. This technique provided a means for depth profiling a thin film since the escape depth of photoelectrons depends on the angle, relative to an axis perpendicular to the film plane, at which they were collected. In a 5 cycle film, where the last growth medium contained Pt^{2+}, the N/Pt ratio was independent of the take-off angle. In a 4.5 cycle film, where the last growth medium contained PAMAM, the N/Pt ratio was larger and decreased sharply with increasing sample depth. These trends showed the outermost dendritic layer was Pt deficient and covered the prior Pt^{2+} bearing layer. This paper demonstrates successful PMF formation between a macromolecule and a metal ion, with alternating metal and polymer layers.

2. Combined Film Preparation Techniques

Lvov describes films assembled with combined SA and Langmuir-Blodgett transfer[33]. The layer composition for the LB films is $(DODAB/PVS/DODAB)_m$.

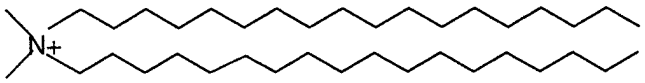

DODAB

LXIII

Through the use of the SA technique, a series of bilayers can be inserted after LB deposition of the PVS layer: $\{DODAB/PVS/(PAH/PVS)_n/DODAB\}_m$. Films with n=0-3 and m=6-10 have been prepared. The films were investigated with SAXR. Variation of the number of PMF bilayers results in a linear increase of the layer spacing of 40Å per inserted bilayer. Heating the samples to 70 °C and slowly cooling resulted in a large improvement in multilayer ordering. Sohling demonstrates the adsorption of dioleoyl-L-α-phosphatidic mono- and bilayers onto a PEI-covered substrate[148]. Films like this have been prepared in the past by the Langmuir-Blodgett technique. By successive adsorption of PEI and phospholipid vesicles, supported bilayers of lipid-polyelectrolyte complexes were prepared.

3. Layer formation by chemical synthesis

By combining *in situ* polymerization of pyrrole with the SA technique, PSS/polypyrrole multilayers have been prepared[30, 74].

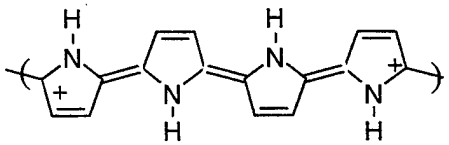

p-Doped Poly(pyrrole)

LXIV

While PSS adsorbed onto a positively charged surface, layers of polypyrrole were formed by dipping a negatively-charged substrate into a solution containing $FeCl_3$, pyrrole monomer and *p*-toluene sulfonic acid. By varying the dip time, the polypyrrole film thickness could be varied in the range 20-60Å. Growth followed zero order kinetics on a negatively charged surface. On positively charged or hydrophobic surfaces, a 20 min induction time appears before polymerization occurs, showing a preference for adsorption onto a negatively charged surface. Multilayers prepared by this procedure had conductivities ranging from 20-80 S/cm, although adjustment in the polymerization chemistry brought the conductivity up to 300 S/cm. PMFs containing uncharged PAn and PSS have been prepared[91]. When doped with HCl the films

become electrically conducting with conductivities comparable to spin-cast films.

A method for preparing noncentrosymmetric films combines electrostatic self assembly and chemical activation[149]. First, an ionene-type polycation was adsorbed onto a surface in the usual manner. The poly cation contained a tertiary aniline residue with which a diazonim salt derived from sodium 2-amino-5-nitrobenzenesulfonate reacts, adding a negatively charged group to the cationic polymer surface and creating a strong dichroic dye containing polymer having a negative charge.

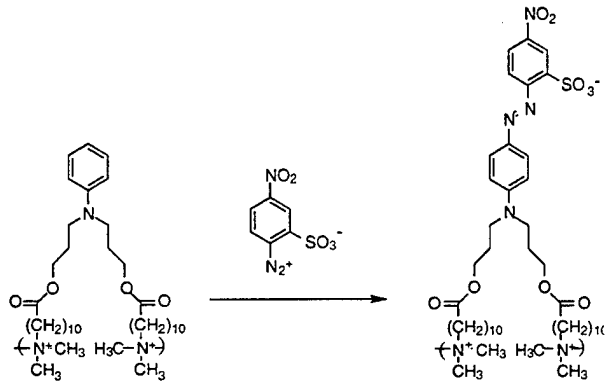

LXV

Following this step another cationic layer was added, forming a multilayer. Second harmonic generation was observed when the films were illuminated with laser radiation, thus confirming noncentrosymmetry.

An example of a using phosphonate multilayers for the preparation of a nonlinear film is described by Katz[150]. He used a three step procedure for preparation of a bilayer. A hydroxy-terminated(The first layer was amine terminated silanized glass.) layer was treated with $POCl_3$, followed by zirconation with $ZrOCl_2$ and treatment with HPP. This cycle was repeated to form a multilayer containing alternating HPP and zirconium phosphate layers(Fig. 21).

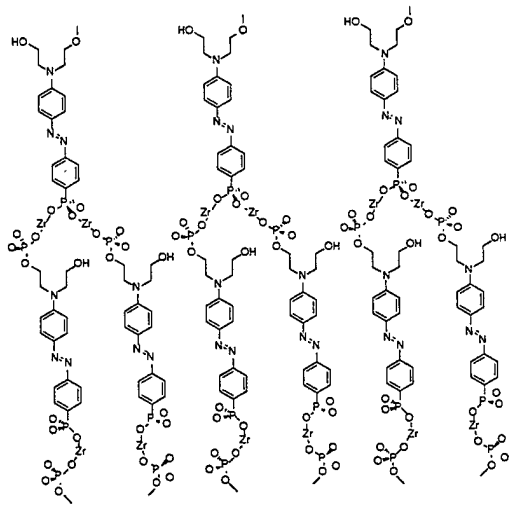

Figure 21. Schematic of nonlinear film based on zirconium phosphate chemistry[150].

Because the chromophores were oriented, the film had NLO activity, showing generation of the second harmonic following irradiation with laser radiation at 1,064 nm.

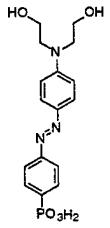

HPP

LXVI

A coordination polymer consisting of Zn and a bisquinoline acceptor has been described[28].

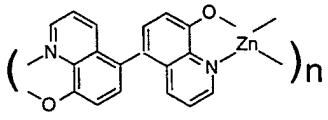

Zn-Bisquinoline

LXVII

When synthesis has been attempted by normal means, the polymer is insoluble. Good quality films were prepared by alternate dipping of the substrate into $Zn(Et)_2$ and bisquinoline THF solutions. The multilayers behaved as light-emitting diodes[151].

4. Premixed Adsorbate Solutions

ESA films prepared with small molecules or rigid components like proteins of inorganic plates often show poor adsorption. A solution to this problem involves pre-mixing of dye molecules and proteins with linear polyions[17]. When a thin film $(PDDA/MY10)_n$ was immersed into a PDDA solution, QCM measurements showed some desorption of the dye.

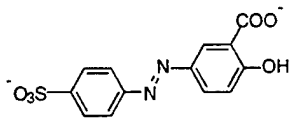

MY10

LXVIII

When the anionic solution contained both MY10 and PSS, thin films having the composition $(PDDA/MY10, PSS)_n$ showed no dye desorption. They also prepared a GOx-containing film. They pre-mixed anionic GOx with cationic PEI and prepared a film $(PEI, GOx/PSS)_n$. The GOx enzyme activity in the modified film was 67 times greater than that of the film $(PEI/GOx)_n$, the increase being due to promotion of a favorable enzyme microenvironment.

V. Future Prospects

The SA technique is a low cost approach for assembling interesting thin films. Virtually any polyion can be incorporated into a film, including dyes, polymers, proteins, viruses, inorganic nanoparticles and ceramic plates. The technique is simple to automate. The SA technique requires minimum equipment investment and interesting films can be made by hand with beakers, electrolytes, water and a stopwatch. By using a moderately-priced automated slide stainer, complex multilayers can be prepared. Compared to the LB technique, scaleup of automated SA film assembly is less costly. This report contains numerous examples of PMFs whose properties can be tuned by varying the number of layers or the spacing between functional layers. Virtually any substrate upon which a charge can be placed can be used in the SA process. The SA process exhibits self-healing characteristics. Point defects and dust inclusions have limited propagation distance. Varying bilayer thickness can be obtained by changing the ionic strength. The SA technique can be combined with other methods(Langmuir-Blodgett technique, spin coating, etc.) to provide a variety of films.

The goal of thin film preparation is the three-dimensional control of film composition and properties according to application requirements. Although the SA technique provides

considerable control of film composition along the Z axis, interpenetration of monolayers is high. Very little work has been done regarding controlling SA film composition in the X and Y axes. The ability of PMF films to be grown on virtually any substrate makes controlling film growth according to a template difficult. Numerous film preparation techniques listed here can potentially be used in combination with the SA technique. Spin coating involves applying a solution of film material to a rapidly spinning disk. A uniform fluid film forms, becoming a solid film after evaporation of the solvent[152-154]. Solvent casting involves placing a polymer solution in a well and evaporating to dryness[155-157]. Films cast in magnetic[158] or electric[159-161] fields yields oriented thin films. Films have been prepared through direct polymerization onto a initiator covalently attached to the substrate[162, 163]. The Langmuir-Blodgett technique involves placing an amphiphile monolayer onto an air-water interface[164]. The water bath has a highly-controlled temperature. A teflon arm touching the interface contains the monolayer and provides a means of measuring and controlling surface pressure. A mechanical dipping apparatus transfers the monolayer onto a glass slide. This process can be repeated many times and complex optical films have been prepared[165]. Practical application of the LB technique has been hindered by the high instrumentation cost and low transfer efficiency[73]. Photolithographic techniques make possible control of molecular structure in the x-y plane. The technique combines solid phase peptide synthesis with semiconductor-based photolithography[166, 167].

This report gives numerous examples of applications where the SA technique could be useful. These applications include light-emitting diode[120], conducting polymer[74], second-order nonlinear optics[124], dye-containing optical film[37, 73, 86, 90, 131], poly(diacetylene)[72], bioreactor[26, 37, 138, 139], molecular recognition by antibody-antigen interaction[20], nonthrombogenic surfaces[34] and nanoscale thin film pH electrode[76]. These results are proof-of-concept studies meriting further advanced development work. The performance of these films needs to be compared with alternative technologies. For example, SA films have the ability to convert starch to gluconic acid[139]. The device is a flow processor with the largest reported reaction rate being 0.0045 mole-$M^{-2}h^{-1}$. In a commercial batch microbial fermenter converting glucose to gluconic acid, the conversion rate is 0.017 mole-$L^{-1}h^{-1}$[168]. A 1 M^2 membrane would have approximately 1/3 the efficiency of a commercial microbial fermenter. Presumably with optimization, the efficiency could reach or exceed the batch system. Also, the SA system is a continuous flow system, with lower cost compared to batch systems. The favorable efficiency suggests SA multienzyme films would be useful for bioreactor applications, especially for preparation of high cost, low quantity specialty materials like pharmaceuticals. Another possible application is the production of light-emitting diodes.

Because they have good light intensity and long term stability, light-emitting diodes prepared by the SA technique appear to be near commercialization[120].

The preparation of films by the SA technique mimics the sequential laying down of protein and calcium carbonate layers observed in biomineralization. Structural hierarchacy analogous to that seen in biology appears in PMFs. A two component film $(AB)_n$ has four levels of structure hierarchy: molecular constituents $\rightarrow$ monolayer $\rightarrow$ bilayer $\rightarrow$ multilayer. A three component film $(ABAC)_n$ film has five levels. With imagination, the reader can conceive of very complex, multicomponent films that could be prepared by this technique. Also, by combining film preparation by other methods(spin coating, Langmuir-Blodgett, etc.), the potential for tailor-making films for specific needs becomes possible.

VI. Acknowledgement

The author thanks Dr. Yuri Lvov for stimulating discussions, assistance in preparing the reference list and practical advice on the technical details of PMF preparation and characterization techniques, Mr. Walt Johnson for optics discussions and Dr. Hao Jiang for XPS data used in Fig. 11.

VII. Abbreviation List

Abbreviation	Name
α-ZrP	α–zirconium phosphate
AR26	Acid Red 26
Bu-PHPyV	poly(2-*n*-butyl-*p*-pyridyl vinylene)
CR	Congo Red
Cu-PTSA	copper phthalocyanine tetrasulfonate
CV	cyclic voltammetry
Cyt	cytochrome
DCDS	10,12-docosadiyne-1,22 disulfate
DIPY08	*p*-phenylenediacrylic acid bis(8-pyridinium-*N*-yl octylester dibromide
DODAB	dimethyldioctyadecylammonium bromide
DPP	1,4-diketo-3,6-diphenylpyrrolo-[3,4-c]-pyrrole sulfonate
FITC-PAH	fluorescein-modified poly(allyl amine)
GA	glucoamylase
GOx	glucose oxidase
Hb	hemoglobin
HPP	4-{4-[*N*,*N*-bis(2-hydroxylethyl)amino]phenylazo}phenylphosphonic acid
IC	Indigo Carmine
IgG	immunoglobulin G
IPEC	interpolyelectrolyte complex
ITO	indium tin oxide
LB	Langmuir-Blodgett
LYS	lysozyme
Mb	myoglobin
MDESA	*p*-methoxy-*N*,*N*-diethyl-2-sulfonic acid

Abbreviation	Name
MINIM	metal-insulator-nanoparticle-insulator-metal
Mont	montmorillonite
MPS	3-mercapto-1-propane sulfonic acid
MV	methyl viologen
MY10	5-(4-sulfophenylazo)salicylic acid disodium salt
PAA	poly(acrylic acid)
PAAm	poly(acrylamide)
PAH	poly(allyl amine)
PAH-Fc	ferrocyne modified poly(allyl amine)
PAM	pentamidine
PAMA	poly(dimethylamino)ethylmethacrylate)
PAMAM	poly(amidoamine) dendrimer
PAMPSA	poly(2-acrylamido-2-methyl-1-propanesulfonic acid)
PAPSA	poly(aniline propane sulfonic acid)
PAZO	poly(1-[4-(3-carboxyl-4-hydroxyphenylazo)benzene sulfonamido]-1,2-ethanediyl, Na salt)
PBV	poly(butanylviologen dibromide)
PCzEMA	poly[2- (9-carbazoly)ethyl methacrylate]
PDDA	poly(dimethyldiallylammonium chloride)
PDNBMA	poly[2-[(3,5-dinitrobenzoyl)oxy)ethyl methacrylate]
PEI	poly(etheleneimine)
PEO	poly(ethylene oxide)
PET	poly(ethylene terephthalate)
PGA	poly(L-glutamic acid)
PLL	poly(L-lysine)
PMA	poly(methacrylic acid)

Abbreviation	Name
PMF	polyion multilayer film
PMPA	poly[(*N*-methyl-pyridinium-2-yl)acetylene
POD	peroxidase
pre-PPV	poly(phenylene vinylene) precursor
PS	Ponceau S
PSMV	poly(styrene, 4-methyl viologen styrene) copolymer
PSS	poly(styrene sulfonate)
PTAA	poly(thiophene acetic acid)
PVA	poly(vinyl alcohol)
PVBT	poly(vinylbenzyltrimethylamine)
PVDA	poly(4-vinylbenzyl-*N,N*-diethyl-*N*-methyl-ammonium iodide)
PVI	poly(vinyl imidazole)
PVP	poly(1-methyl-2-vinylpyridinium)
PVP	poly(vinyl pyrrolidone)
PVPC	(1-ethyl-4-vinylpyridinium)-vinylpyridine copolymer
PVPMe	poly(4-vinyl-1-methyl-pyridinium methyl sulfate)
PVRu	poly(4-methyl, 4'-vinyl-bipyridine-bisbipyridine ruthenium)
PVS	poly(vinyl sulfate)
QCM	quartz crystal microbalance
SA	sequential adsorption
SAXR	small angle X-ray reflection
SPAn	sulfonated poly(aniline)
TBA	tetra N-butyl ammonium
TIRF	total internal reflection fluorescence
TMPyP	α,β,γ,δ-tetrakis(1-*N*-methylpyridyl)porphine

Abbreviation	Name
TPPS	tetraphenylporphine sulfonate
XPS	X-ray photoelectron spectroscopy
ZnTPyBBCR	zinc-tetrakis[bispyridine)(chloro)ruthenium] porphine

VIII. References

1. M. Sarikaya and I. A. Aksay(eds.). *Biomimetics: Design and Processing of Materials*, AIP Press, Woodbury, (1995).

2. M. Alper, H. Bayley, D. Kaplan and M. Navia, *Biomolecular Materials by Design*, MRS Symp. Proc. **330**, (1994).

3. A. H. Heuer, D. J. Fink, V. J. Laraia, J. L. Arias, P. D. Calvert, K. Kendall, G. L. Messing, J. Blackwell, P. C. Rieke, D. H. Thompson, A. P. Wheeler, A. Veis and A. I. Caplan *Science* **255**, 1098, (1992).

4. B. S. Thompson *SAMPE J.* **32**, 38, (1996).

5. E. A. Di Marzio *MRS Symp. Proc.* **255**: 333 (1992).

6. D. A. Tirrell(ed.) (1994) *Hierarchical structures in biology as a guide for new materials technology*, National Academy Press, Washington D.C., (1994).

7. G. Decher *Science* **277**, 1232, (1997).

8. J. H. Fendler *Chem. Mater.* **8**, 1616, (1996).

9. Y. M. Lvov and G. Decher *Crystallography Reports* **39**, 696, (1994).

10. M. Sano, Y. Lvov and T. Kunitake *Ann. Rev. Mater. Sci.* **26**, 153, (1996).

11. V. V. Tsukruk *Prog. Polym. Sci.* **22**, 247, (1997).

12. P. Hammond and G. Whitesides *Macromolecules* **28**, 7569, (1995).

13. A. Delcorte, P. Bertrand, X. Arys, A. Jonas, E. Wischerhoff, B. Mayer and A. Laschewsky *Surf. Sci.* **366**, 149, (1996).

14. Y. Lvov, M. Onda, K. Ariga and T. Kunitake *J. Biomater. Sci.* **in press**, (1997).

15. Y. Lvov, K. Ariga, I. Ichinose and T. Kunitake *Langmuir* **12**, 3038, (1996).

16. X. Zhang, Y. Sun, M. Gao, X. Kong and J. Shen *Macromol. Chem. Phys.* **197**, 509, (1996).

17. K. Ariga, M. Onda, Y. Lvov and T. Kunitake *Chem. Lett.* 25, (1997).

18. W. Chen and T. McCarthy *Macromolecules.* **30**, 78, (1997).

19. G. Mao, Y. Tsao, M. Tirrell, H. Davis, V. Hessel and H. Ringsdorf *Langmuir* **11**, 942, (1995).

20. F. Caruso, K. Niikura, N. Furlong and Y. Okahata *Langmuir* **13**, 3427, (1997).

21. R. Advincula, E. Aust, W. Meyer and W. Knoll *Langmuir* **12**, 3536, (1996).

22. N. Hoogeveen, M. Stuart and G. Fleer *Langmuir* **12**, 3675, (1996).

23. E. Kleinfeld and G. Ferguson *Chem. Mater.* **8**, 1575, (1996).

24. D. Ingersoll, P. Kulesza and L. Faulkner *J. Electrochem. Soc.* **141**, 140, (1994).

25. F. Saremi, E. Maassen, B. Tieke, G. Jordan and W. Rammensee *Langmuir* **11**, 1068, (1995).

26. J. Hodak, R. Etchenique, E. Calvo, K. Singhal and P. Bartlett *Langmuir* **13**, 2708, (1997).

27. W. Kong, L. Wang, M. Gao, H. Zhou, X. Zhang, W. Li and J. Shen *J. Chem. Soc. Chem. Commun.* 1297, (1994).

28. D. L. Thomsen and F. Papadimitrakopoulos *Polymer Preprints* **38**, 355, (1997).

29. J. Tian, C. Wu, M. Thompson, J. Sturm, R. Register, M. Marsella and T. Swager *Adv. Mater.* **7**, 395, (1995).

30. J. Cheung, A. Fou and M. Rubner *Thin Solid Films* **244**, 985, (1994).

31. S. W. Keller, H. N. Kim and T. E. Mallouk *J. Am. Chem. Soc.* **116**, 8817, (1994).

32. D. L. Feldheim, K. C. Grabar, M. J. Natan and T. E. Mallouk *J. Am. Chem. Soc.* **118**, 7640, (1996).

33. Y. Lvov, F. Essler and G. Decher *J. Phys. Chem.* **97**, 13773, (1993).

34. M. Houska and E. Brynda *J. Coll. Interface Sci.* **188**, 243, (1997).

35. H. Fan, Y. Zhou and G. Lopez *Adv. Mater.* **9**, 728, (1997).

36. R. Klitzing and H. Mohwald *Langmuir* **11**, 3554, (1995).

37. Y. Sun, X. Zhang, C. Sun, B. Wang and J. Shen *Macromol. Chem. Phys.* **197**, 147, (1996).

38. T. M. Cooper, A. L. Campbell and R. L. Crane *Langmuir* **11**, 2713, (1995).

39. J. Hong, K. Lowack, J. Schmitt and G. Decher *Prog. Colloid Polymer Sci.* **93**, 98, (1993).

40. D. Pum, M. Sara and U. B. Sleytr *J. Vac. Sci. Technol B* **7**, 1391, (1989).

41. J. Engel in *Biophysics* , W. Hoppe, W. Lohmann, H. Markl and H. Ziegler (ed.). Springer-Verlag, Berlin(1983), pp. 408-412.

42. T. M. Cooper and R. W. Woody *Biopolymers* **30**, 657, (1990).

43. A. D. MacLachlan and M. Stewart *J. Mol. Biol.* **103**, 271, (1976).

44. D. Cabral-Lilly, G. N. Philips, G. E. Sosinsky, L. Melanson, S. Chacko and C. Cohen *Biophys. J.* **59**, 805, (1991).

45. D. L. D. Caspar, C. Cohen and W. Longley *J. Mol. Biol.* **41**, 87, (1969).

46. S. I. Stupp, S. Son, L. S. Li, H. C. Lin and M. Keser *J. Am. Chem. Soc.* **117**, 5212, (1995).

47. S. I. Stupp, S. Son, H. C. Lin and L. S. Li *Science* **259**, 59, (1993).

48. L. H. Radzilowski, B. O. Carragher and S. I. Stupp *Macromolecules* **30**, 2110, (1997).

49. S. I. Stupp, V. LeBonheur, K. Walker, L. S. Li, K. E. Huggins, M. Keser and A. Arnstutz *Science* **276**, 384, (1997).

50. V. A. Kabanov *Polym. Sci.* **36**, 143, (1994).

51. H. Ghiradella *Ann. Entomol. Soc.* **77**, 637, (1984).

52. C. W. Mason *J. Phys. Chem.* **30**, 383, (1926).

53. C. W. Mason *J. Phys. Chem.* **31**, 321, (1927).

54. C. W. Mason *J. Phys. Chem.* **31**, 1856, (1927).

55. H. Ghiradella *Appl. Opt.* **30**, 3492, (1991).

56. H. Ghiradella *J. Morphology* **142**, 395, (1974).

57. H. Ghiradella, D. Aneshansley, T. Eisner, R. E. Silberglied and H. E. Hinton *Science* **178**, 1214, (1972).

58. H. Ghiradella *J. Morphology* **202**, 69, (1989).

59. K. S. Gould and D. W. Lee *Amer. J. Bot.* **83**, 45, (1996).

60. R. M. Graham, D. W. Lee and K. Norstog *Amer. J. Bot.* **80**, 198, (1993).

61. D. W. Lee, R. A. Bone, S. L. Tarsis and D. Storch *Amer. J. Bot.* **77**, 370, (1990).

62. D. W. Lee *Nature* **349**, 260, (1991).

63. C. M. Zaremba, A. M. Belcher, M. Fritz, Y. Li, S. Mann, P. K. Hansma, D. E. Morse, J. S. Speck and G. D. Stucky *Chem. Mater.* **8**, 679, (1996).

64. A. M. Belcher, X. H. Wu, R. J. Christensen, P. K. Hansma, G. D. Stucky and D. E. Morse *Nature* **381**, 56, (1996).

65. M. A. Cariolou and D. E. Morse *J. Comp. Physiol. B* **157**, 717, (1988).

66. G. Falini, S. Albeck, S. Weiner and L. Addadi *Science* **271**, 67, (1996).

67. T. E. Schaffer, C. Ionescu-Zanetti, R. Proksch, M. Frita, D. A. Walters, N. Almqvist, C. M. Zaremba, A. M. Belcher, B. L. Smith, G. D. Stucky, D. E. Morse and P. K. Hansma *Chem. Mater.* **9**, 1731, (1997).

68. J. Lin, E. Cates and P. Bianconi *J. Am. Chem. Soc.* **116**, 4738, (1994).

69. R. K. Iler *J. Colloid and Interface Sci.* **21**, 569, (1966).

70. R. K. Iler, U.S. Patent No. 3,485,658, (1969).

71. D. Laurent and J. Schlenoff *Langmuir* **13**, 1552, (1997).

72. F. Saremi and B. Tieke *Adv. Mater.* **7**, 378, (1995).

73. K. Ariga, Y. Lvov and T. Kunitake *J. Am. Chem. Soc.* **119**, 2224, (1997).

74. A. C. Fou and M. F. Rubner *Macromolecules* **28**, 7115, (1995).

75. F. Caruso, K. Niikura, D. N. Furlong and Y. Okahata *Langmuir* **13**, 3422, (1997).

76. D. Lowy and H. Finklea *Electrochimica Acta* **42**, 1325, (1997).

77. G. B. Sukhorukov, J. Schmitt and G. Decher *Ber. Bunsenges. Phys. Chem.* **100**, 948, (1996).

78. E. R. Kleinfeld and G. S. Ferguson *Science* **265**, 370, (1994).

79. Y. Lvov, H. Haas and G. Decher *J. Phys. Chem.* **97**, 12385, (1993).

80. G. Decher, J. D. Hong and J. Schmitt *Thin Solid Films* **210**, 831, (1992).

81. Y. Lvov, K. Ariga, I. Ichinose and T. Kunitake *J. Amer. Chem. Soc.* **117**, 6117, (1995).

82. G. Mao, Y. Tsao, M. Tirrell, H. T. Davis, V. Hessel and H. Ringsdorf *Langmuir* **9**, 3461, (1993).

83. J. Schmitt, T. Grunewald, G. Decher, P. Pershan, K. Kjaer and M. Loscge *Macromolecules* **26**, 7058, (1993).

84. N. A. Kotov, I. Dekany and J. H. Fendler *J. Phys. Chem.* **99**, 13065, (1995).

85. J. J. Ramsden, Y. M. Lvov and G. Decher *Thin Solid Films* **254**, 246, (1995).

86. K. Araki, M. J. Wagner and M. S. Wrighton *Langmuir* **12**, 5393, (1996).

87. W. Kong, X. Zhang, M. L. Gao, H. Zhou, W. Li and J. Shen *Macromol. Rapid. Commun.* **15**, 405, (1994).

88. Y. Lvov, G. Decher and H. Mohwald *Langmuir* **9**, 481, (1993).

89. Y. Lvov, H. Haas, G. Decher, H. Mohwald, A. Mikhailov, B. Mtchedlishvily, E. Morgunova and B. Vainshtein *Langmuir* **10**, 4232, (1994).

90. D. Yoo, J. Lee and M. F. Rubner *Mat. Res. Soc. Symp. Proc.* **413**, 395, (1996).

91. J. H. Cheung, W. B. Stockton and M. F. Rubner *Macromolecules* **30**, 2712, (1997).

92. G. Decher, Y. Lvov and J. Schmitt *Thin Solid Films* **244**, 772, (1994).

93. B. Lehr, M. Seufert, G. Wenz and G. Decher *Supramol. Sci.* **2**, 199, (1995).

94. A. Krozer, S. Nordin and B. Kasemo *J. Coll. Interface Sci.* **176**, 479, (1995).

95. Y. Lvov, K. Ariga, M. Onda, I. Ichinose and T. Kunitake *Lamgmuir* **In Press**, (1997).

96. T. P. Russell *Mat. Sci. Reports.* **5**, 171, (1990).

97. M. Ferreira, J. H. Cheung and M. F. Rubner *Thin Solid Film* **244**, 806, (1994).

98. R.M.A. Azzam and N.M. Bashare, *Ellipsometry and Polarized Light* , North-Holland, Amsterdam(1987).

99. H.G. Tompkins *A User's Guide to Ellipsometry* , Academic Press, Boston(1993).

100. B. Sellergren, A. Swietlow, T. Amebrant and K. Unger *Anal. Chem.* **68**, 402, (1996).

101. R. Klitzing and H. Mohwald *Thin Solid Films* **284-285**, 352, (1996).

102. J. G. Gordon and J. D. Swalen *Opt. Commun.* **22**, 374, (1977).

103. Y. Shimizaki, M. Mitsuishi, S. Ito and M. Yamamoto *Langmuir* **13**, 1385, (1997).

104. B. Bhushan, J. Israelachvili and U. Landman *Nature* **374**, 607, (1995).

105. J. Frommer *Angew. Chem. Int. Ed. Engl.* **31**, 1298, (1992).

106. V. V. Tsukruk and D. H. Reneker *Polymer* **36**, 1791, (1995).

107. C. D. Frisbie, L. F. Rozsnai, A. Noy, M. S. Wrighton and C. M. Lieber *Science* **265**, 2071, (1994).

108. V. N. Bliznyuk, D. W. Visser, V. V. Tsukruk, A. L. Campbell, T. Bunning and W. W. Adams *Polymer Preprints* **37**: 608 (1996).

109. C. A. Johnson and A. M. Lenhoff *J. Coll. Interface Sci.* **179**, 587, (1996).

110. G. Sauerbry *Z. Phys.* **155**, 206, (1959).

111. A. Adamson *Physical Chemistry of Surfaces* , John Wiley and Sons, New York(1982).

112. M. Murray and B. Darvell *J. Phys D: Appl. Phys.* **23**, 1150, (1990).

113. Y. Liu, A. Wang and R. Claus *J. Phys. Chem. B* **101**, 1385, (1997).

114. H. S. Munro and S. Singh in *Polymer Characterisation* , B. J. Hunt and M. I. James (eds.) Blackie Academic and Professional, London(1993), 333.

115. G. Decher and J. Schmitt *Prog. Coll. Polymer Sci.* **89**, 160, (1992).

116. T. Cosgrove, T. M. Obey and B. Vincent *J. Colloid Interface Sci.* **111**, 409, (1986).

117. P. Stroeve, V. Vasquez, M. Coelho and J. Rabolt *Thin Solid Films* **284-285**, 708, (1996).

118. J. Lavasalmi and T. McCarthy *Macromolecules* **30**, 1752, (1997).

119. M. Ferreira and M. F. Rubner *Macromolecules* **28**, 7107, (1995).

120. A. C. Fou, O. Onitsuka, M. Ferreira and M. F. Rubner *J. Appl. Phys.* **79**, 7501, (1996).

121. M. Onoda and K. Yoshino *Jpn. J. Appl. Phys.* **34**, L260, (1995).

122. O. Onitsuka, A. C. Fou, M. Ferreira, B. R. Hsieh and M. F. Rubner *J. Appl. Phys.* **80**, 406, (1996).

123. V. Tsukruk, F. Rinderspacher and V. Bliznyuk *Langmuir* **13**, 2171, (1997).

124. Y. Lvov, S. Yamada and T. Kunitake *Thin Solid Films* **300**, 107, (1997).

125. G. Decher and J. Hong (1991). *Makromol. Chem., Macromol. Symp.* **46**: 321 (1991).

126. G. Decher and J. D. Hong *Ber. Bunsenges. Phys. Chem.* **95**, 1430, (1991).

127. M. Gao, X. Kong, X. Zhang and J. Shen *Thin Solid Films* **244**, 815, (1994).

128. X. Zhang, M. Gao, X. Kong, Y. Sun and J. Shen *J. Chem. Soc. Chem. Commun.* 1055, (1994).

129. C. Sun, X. Zhang, D. Jiang, Q. Gao, H. Xu, Y. Sun, X. Zhang and J. Shen *J. Electroanalytical Chemistry* **411**, 73, (1996).

130. C. Sun, Y. Sun, X. Zhang, H. Xu and J. Shen *Analyt. Chim. Acta* **312**, 207, (1995).

131. F. Saremi, G. Lange and B. Tieke *Adv. Mater.* **8**, 923, (1996).

132. G. Decher, F. Essler, J. Hong, K. Kowack, J. Schmitt and Y. Lvov *Polym. Preprints* **34**, 745, (1993).

133. Y. Lvov, G. Decher and H. Mohwald *Macromolecules* **26**, 5396, (1993).

134. T. M. Cooper, A. L. Campbell, C. Noffsinger, J. Gunther-Greer, R. L. Crane and W. W. Adams *MRS Proceedings* **351**, 239, (1994).

135. Y. Lvov, K. Ariga, I. Ichinose and T. Kunitake *Thin Solid Films* **284-285**, 797, (1996).

136. Y. Lvov, K. Ariga and T. Kunitake *Chem. Lett.* 2323, (1994).

137. J. Glenn and E. Bowden *Chem. Lett.* 399, (1996).

138. M. Onda, Y. Lvov, K. Ariga and T. Kunitake *Biotech. Bioeng.* **51**, 163, (1996).

139. M. Onda, Y. Lvov, K. Ariga and T. Kunitake *J. Ferment. Bioeng.* **82**, 502, (1996).

140. K. Ariga, Y. Lvov, M. Onda, I. Ichinose and T. Kunitake *Chem. Lett.* 125, (1997).

141. J. Schmidt, G. Decher, W. J. Dressick, S. L. Brandow, R. E. Geer, R. Shashidhar and J. M. Calvert *Adv. Mater.* **9**, 61, (1997).

142. M. Gao, M. Gao, X. Zhang, Y. Yang, B. Yang and J. Shen *J. Chem. Soc. Chem. Commun.* 2777, (1994).

143. M. Gao, X. Zhang, B. Yang, F. Li and J. Shen *Thin Solid Films* **284-285**, 242, (1996).

144. G. Cao, H. Hong and T. E. Mallouk *Acc. Chem. Res.* **25**, 420, (1992).

145. S. W. Keller, S. A. Johnson, E. S. Brigham, E. H. Yonemoto and T. E. Mallouk *J. Am. Chem. Soc.* **117**, 12879, (1995).

146. W. B. Stockton and M. F. Rubner *Macromolecules* **30**, 2717, (1997).

147. S. Watanabe and S. L. Regen *J. Am. Chem. Soc.* **116**, 8855, (1994).

148. U. Sohling and A. Schouten *Langmuir* **12**, 3912, (1996).

149. A. Laschewsky, B. Mayer, E. Wischerhoff, X. Arys, P. Bertrand, A. Delcorte and A. Jonas *Thin Solid Films* **284-285**, 334, (1996).

150. H. E. Katz, G. Scheller, T. M. Putvinski, M. L. Schilling, W. L. Wilson and C. E. D. Chidsey *Science* **254**, 1485, (1991).

151. D. Thomsen, K. Higginson and F. Papadimitrakopoulos *Polymer Preprints* **38**, 353, (1997).

152. T. M. Cooper, A. L. Campbell, W. Su, K. Obermeier, K. Natarajan, R. L. Crane, W. W. Adams and M. Brant *MRS Symp. Proc.* **374**, 99, (1995).

153. W. A. Levinson, A. Arnold and O. Dehodgins *Polymer Engineering and Science* **33**, 980-988, (1993).

154. D. Meyerhofer *J. Appl. Phys.* **49**, 3993, (1978).

155. A. J. McKinnon and A. V. Tobolsky *J. Phys. Chem.* **70**, 1453, (1966).

156. A. J. McKinnon and A. V. Tobolsky *J. Phys. Chem.* **72**, 1157, (1968).

157. A. V. Tobolsky and E. T. Samulski *Adv. Chem. Phys.* **21**, 529, (1971).

158. E. T. Samulski and A. V. Tobolsky *Macromol.* **1**, 555, (1968).

159. E. Iizuka *Biochim. Biophys. acta.* **175**, 457, (1969).

160. D. J. Trantolo, J. D. Gresser, D. L. Wise, M. G. Mogul, T. M. Cooper and G. E. Wnek *SPIE Proceedings* **2528**, 219, (1995).

161. C. G. Worley, R. W. Linton and E. T. Samulski *Langmuir* **11**, 3805, (1995).

162. J. K. Whitesell and H. K. Chang *Science* **261**, 73, (1993).

163. R. H. Wieringa and A. J. Schouten *Macromolecules* **29**, 3032, (1996).

164. H. Fuchs, H. Ohst and W. Prass *Adv. Mater.* **3**, 10, (1991).

165. N. Carr in *Special Polymers for Electronics and Optoelectronics* , and J.A. Chilton and M.T. Goosey(eds.)., Chapman and Hall, London(1995), pp. 81-130.

166. S. P. A. Fodor, J. L. Read, M. C. Pirrung, L. Stryer, A. T. Lu and D. Solas *Science* **251**, 767, (1991).

167. J. W. Jacobs and S. P. A. Fodor *Trends in Biotechnology* **12**, 19, (1994).

168. B. Atkinson and F. Mavituna(eds.). *Biochemical Engineering and Biotechnology Handbood Second Ed.*, Stockton Press, New York(1991).

169. D. Korneev, Y. Lvov, G. Decher, J. Schmitt and S. Yaradaikin *Physica B* **213**, 954, (1995).

170. Y. Lvov, G. Decher, H. Haas, H. Mohwald and A. Kalachev *Physica B* **198**, 89, (1994).

Distribution List

DET 1 AFRL/WST
2690 C STREET STE 4
WRIGHT-PATTERSON AFB OH 45433-7411

DR THOMAS COOPER
AFRL/MLPJ
BLDG 651 RM 169
3005 P STREET
WRIGHT-PATTERSON AFB OH 45433-7702

AFRL/MLPJ
HMTEC
3005 P STREET RM 169
WRIGHT-PATTERSON AFB OH 45433-7702

DR JEFFREY F DENATALE
ROCKWELL INTERNATIONAL SCIENCE CENTER
SCIENCE CENTER
1049 CAMINO DOS RIOS
THOUSAND OAKS CA 91360

DEFENSE TECHNICAL INFORMATION CENTER
DTIC/OMI
8725 JOHN J KINGMAN ROAD SUITE 0944
FT BELVOIR VA 22060-6218

DR GEORGE P MUELLER
DEPARTMENT OF THE NAVY
NAVAL RESEARCH LABORATORY
CODE 6336
4555 OVERLOOK AVENUE SW
WASHINGTON DC 20375

USAF AIR LIBRARY
AUL/LSAD
600 CHENNAULT CIRCLE
MAXWELL AFB AL 36112-6424

MR BYONG H AHN
US ARMY
NVESD
10221 BURBECK RD STE 430
FT BELVOIR VA 22060-5806